Transmission Line EMTP Models Influence on Time-Domain Fault Location and Protection Functions During Performance Assessment Tests

LUIZA MENDONÇA AVIANI RIBEIRO

MASTER THESIS
ON ELECTRICAL ENGINEERING

ELECTRICAL ENGINEERING DEPARTMENT

TECHNOLOGY FACULTY

UNIVERSITY OF BRASÍLIA

Universidade de Brasília
Faculdade de Tecnologia
Departamento de Engenharia Elétrica

Transmission Line EMTP Models Influence on Time-Domain Fault Location and Protection Functions During Performance Assessment Tests

Luiza Mendonça Aviani Ribeiro

DISSERTAÇÃO DE MESTRADO SUBMETIDA AO PROGRAMA DE PÓS-GRADUAÇÃO EM ENGENHARIA ELÉTRICA DA UNIVERSIDADE DE BRASÍLIA COMO PARTE DOS REQUISITOS NECESSÁRIOS PARA A OBTENÇÃO DO GRAU DE MESTRE.

APROVADA POR:

Prof. Felipe Vigolvino Lopes, D.Sc. (DEE-UFPB)
(Orientador)

Profa. Núbia Silva Dantas Brito, (DEE-UFCG)
(Examinadora Externa)

Prof. Kleber Melo e Silva, D.Sc. (ENE-UnB)
(Examinador Interno)

Brasília/DF, dezembro de 2021.

FICHA CATALOGRÁFICA

RIBEIRO, LUIZA MENDONÇA AVIANI

Transmission Line EMTP Models Influence on Time-Domain Fault Location and Protection Functions During Performance Assessment Tests. [Distrito Federal] 2021.

xvi, 134p., 210 x 297 mm (ENE/FT/UnB, Mestre, Dissertação de Mestrado, 2021).

Universidade de Brasília, Faculdade de Tecnologia, Departamento de Engenharia Elétrica.

Departamento de Engenharia Elétrica

1. ATP/EMTP
2. Traveling Wave Theory
3. Fault Location
4. Protection Function
5. Line model parameters
6. Transposition schemes
7. Soil heterogeneity
8. Transmission lines

I. ENE/FT/UnB

II. Título (série)

REFERÊNCIA BIBLIOGRÁFICA

RIBEIRO, L. M. A. (2021). Transmission Line EMTP Models Influence on Time-Domain Fault Location and Protection Functions During Performance Assessment Tests. Dissertação de Mestrado em Engenharia Elétrica, Publicação PPGEE.DM-780/22, Departamento de Engenharia Elétrica, Universidade de Brasília, Brasília, DF, 134p.

CESSÃO DE DIREITOS

AUTOR: Luiza Mendonça Aviani Ribeiro

TÍTULO: Transmission Line EMTP Models Influence on Time-Domain Fault Location and Protection Functions During Performance Assessment Tests.

GRAU: Mestre ANO: 2021

Luiza Mendonça Aviani Ribeiro

Universidade de Brasília (UnB)

Campus Darcy Ribeiro

Faculdade de Tecnologia - FT

Departamento de Eng. Elétrica (ENE)

Brasília - DF CEP 70919-970

ACKNOWLEDGEMENTS

Firstly, I would like to thank my parents Laura and Cássio, as well as my brother Vitor, for all their support and encouragement in all my decisions. Thank you for all teachings, fellowship and love throughout my trajectory.

I am extremely thankful to my advisor Dr. Felipe Lopes for giving me the opportunity to work on this master thesis. Thank you for the constant encouragement, support and guidance given to me during this period. It has been an honor and a pleasure to have him as my advisor.

To Gustavo Cunha, Eduardo Ribeiro, Amauri Martins-Britto and Felipe Lopes, I give my heartfelt thanks for the fruitful discussions, valuable suggestions and friendship throughout this project, which were essential and inspiring for my academic and professional life. I am thankful to Leticia Gama and all my LAPSE colleagues for all their help and teachings.

To my friends Fernanda Nunes, Leticia Lima, Caio Martins, Murilo Botelho, Gustavo Leão, Guilherme Raposo, Ana Flávia Castro, Diogo Eira, Eduardo Sanchez, Geovanna Gravia and Giovana Travassos, my sincere gratitude for all the shared moments, talks and patience. Thank you for your friendship.

To Clara Outeiral and Natália Vieira, with whom I shared not only many good and bad moments, but also the same house, I thank you for the crazy times, but mainly for the love and the supportive moments. To my lifelong friends, Clara Martins and Paula Medeiros, thank you for the continued companionship and the love, even from afar. Finally, I am greatly thankful to my friend Matheus Amaral for the support, encouragement and fellowship through this year.

To CAPES, thanks for the financial support provided during this master thesis.

RESUMO

Este trabalho apresenta uma série de análises de simulações do tipo *Electromagnetic Transients Program* (EMTP) acerca de padrões de propagação de transitórios oriundos de faltas em linhas de transmissão (LT). Esses transitórios são tipicamente conhecidos por ondas viajantes (OV) e podem apresentar diferentes características em testes EMTP quando considerados diferentes modelos de LT. Diferentes sistemas de potência são modelados e simulados no *software Alternative Transients Program* (ATP), considerando modelos de linha com parâmetros dependentes e independentes da frequência; linhas idealmente transpostas e com simulação de transposição real; e linhas com resistividade do solo homogênea ou heterogênea. Assim, os efeitos causados por essas características na precisão de algoritmos de proteção presentes em relé no domínio do tempo e de localização de falta baseados em OV e em impedância (Z) são avaliados. Para tanto, realizam-se simulações e análises em massa, identificando o padrão de transitório gerado que se assemelha mais com registros reais de faltas. Adicionalmente, observa-se que para algoritmos baseados em OV, modelagens mais complexas apresentam em geral cenários mais adversos para a localização de faltas precisa. Por fim, comparações de desempenho das funções presentes no relé para cada sistema também são apresentadas, evidenciando impactos mais relevantes dos modelos EMTP em relação aos procedimentos de identificação da onda refletida do ponto de falta, especialmente em quando consideradas faltas com conexão para o solo e linhas com transposição real modelada.

Palavras-chave: Modelagem de linha de transmissão, localização de faltas, proteção no domínio do tempo, esquemas de transposição, dependência da frequência dos parâmetros, heterogeneidade do solo.

ABSTRACT

This work analyzes a set of Electromagnetic Transients Program (EMTP) simulations of transmission line (TL) fault transients propagation patterns. These fault transients are well-known as traveling waves (TW), and they can present different features in EMTP testing simulations when different line models are considered. Several power systems are modeled and simulated at Alternative Transients Program (ATP), accounting for lines modeled as frequency-dependent and independent parameters; ideally transposed lines and using real transposition scheme; and homogeneity and heterogeneity soil resistivity. Thereby, the effects of these characteristics on the accuracy of TW- and impedance (Z)-based fault location and protection functions embedded in a time-domain relay are assessed. To do so, massive simulations and studies are carried out, identifying the induced transients patterns most similar to those verified in real-world scenarios. In addition, it is observed that for TW-based algorithms, realistic TL modeling yield, in general, more challenging scenarios for accurate fault location procedures. Besides, the relay functions performance comparisons for each system are presented, highlighting the most relevant impacts caused by different EMTP line models on the detection of TW reflected from the fault point, specially when grounded faults are considered or when the real transposition scheme is modeled.

Keywords:

Transmission line modeling, fault location, time-domain protection, transposition schemes, frequency-dependence parameters, soil heterogeneity.

TABLE OF CONTENTS

LIST OF FIGURES

LIST OF TABLES

LIST OF SYMBOLS

C	Line capacitance
c	Speed of light
d	Fault distance in km
G	DS filter gain
$I_{2\mathrm{L}}$	Negative-sequence current fault contribution in terms of the local bus
$I_{2\mathrm{R}}$	Negative-sequence current fault contribution in terms of the remote bus
I_{LP}	Loop current phasor
I_{OP}	Operation current
I_{POL}	Polarizing current
I_{RTL}	Current restraining variable for local bus
I_{RTR}	Current restraining variable for remote bus
I_{TW}	Current TW amplitude
I_{TWL}	Incident current TW at local terminal
I_{TWR}	Incident current TW at remote terminal
I_z	Non-incremental replica current
L	Line inductance
l	Line length
N_{DS}	DS filter coefficients number
m_0	Protection reaching point
p	Number of cycles

P	Time difference between current TWs arrival time at both ends
R_f	Fault resistance
s	Instantaneous measured signal
t	Time
$t1_1$	Incident TW at local terminal
$t1_3$	Reflected TW at local terminal
$t1_4$	Refracted TW at local terminal
$t2_1$	Incident TW at remote terminal
$t2_4$	Reflected TW at remote terminal
T	Signal fundamental period
T_{OP}	Operating torque
TW_A	Input phase-A signal
TW_B	Input phase-B signal
TW_C	Input phase-C signal
v_{pTW}	TW propagation speed
V	Voltage
V_f	Pre-fault voltage
V_{LP}	Loop voltage phasor
$V_{2\mathrm{L}}$	Negative-sequence voltage fault contribution in terms of the local bus
$V_{2\mathrm{R}}$	Negative-sequence voltage fault contribution in terms of the remote bus
$V_{21\mathrm{OP}}$	Operation voltage from TD21
$V_{21\mathrm{R}}$	Restriction voltage from TD21
V_{TW}	Voltage TW amplitude
Z_1	TL positive-sequence impedance

Z_s	Surge impedance
Z_{TL}	Positive-sequence line impedance
τ	TW propagation time
θ	Fault inception angle
ρ_e	Soil resistivity
ΔI_z	Incremental replica current
Δs	Instantaneous incremental-quantity
ΔV	Incremental voltage

GLOSSARY

A/D	Analog - Digital
AG	Single-Phase-A-to-Ground Fault
ANEEL	Agência Nacional de Energia Elétrica
ATP	Alternative Transients Program
BC	Double-Phase-BC Fault
Be	Bergeron line model
C1T	Classical One-Terminal Method
C2T	Classical Two-Terminal Method
CT	Current Transform
CVT	Capacitor Voltage Transform
DETWFL	Double-Ended TW-based Fault Location Method
DEZFL	Double-Ended Z-based Fault Location Method
DS	Differentiator-Smoother
DTT	Direct Transfer Tripp
DWT	Discrete Wavelet Transform
EMTP	Electromagnetic Transients Program
EPE	Empresa de Pesquisa Energética
EPS	Electrical Power System
FC	Fundamental Components
FIR	Finite Impulse Response

FLO	Settings-Free Two-Terminal Asynchronous Method
GIL	Settings-Free Two-Terminal Method
HS	Homogeneous Soil
IdT	Ideally Transposed line
IED	Intelligent Electronic Devices
IQ	Incremental-Quantity
JM	J.Marti model line
LCC	ATP Line Constants block routine
MODWT	Maximal Overlapped Discrete Wavelet Transform
NHS	Non-Homogeneous Soil
OC21	Overcurrent element
ONS	Operador Nacional do Sistema Elétrico
PDE	Plano Decenal de Expanção de energia
POTT	Permissive Overreaching Transfer Trip
SEL	Schweitzer Engineering Laboratories
SETWFL	Single-Ended TW-based Fault Location Method
SEZFL	Single-Ended Z-based Fault Location Method
SM	Security Margin
T	Transposed line
TD21	Time-Domain 21
TD32	Time-Domain 32
TDQ	Park's Transformation
TL	Transmission Line
TW	Traveling Wave

TW0	Zero Mode Traveling Wave
TW1	Alpha Mode Traveling Wave
TW2	Beta Mode Traveling Wave
TW32	Traveling Wave 32
TW87	Traveling Wave 87
TWFL	Traveling Wave-Based Fault Location
UnT	Untransposed line
VT	Voltage Transform
Z	Impedance
Z1MAG	Positive-Sequence Line Magnitude Impedance
Z1ANG	Positive-Sequence Line Angle Impedance
Z0MAG	Zero-Sequence Line Magnitude Impedance
Z0ANG	Zero-Sequence Line Angle Impedance

CHAPTER 1

INTRODUCTION

1.1 CONTEXTUALIZATION

Since the early stages of electricity, the world is becoming increasingly dependent on electric power. Nowadays, the economy, politics and health care cannot work without energy. Since it has considered a critical infrastructure and a society need, problems in the power grid can spread out very quickly. For instance, in November 2020, a blackout occurred in Amapá, a city in Brazil, led the city to run out of power energy for a few days (ONS, 2020).

The high dependence of electricity require plan actions to minimize problems in the correct functioning of the electric sector, ensuring quality, continuity, and reliability in the supply of energy to the country. It mainly impacts the industrial economy and population growth, such that the electric power consumption per capita is today of about 1.5% p.a. in the country (EPE, 2021).

Aiming to cover all the growing electric energy demand, it becomes fundamental to expand the electric grid. In this context, transmission lines (TL) are of utmost importance, since they make provide the interconnection between generation plants in distant areas and load centers. For this purpose, the Energy Research Office (EPE in Portuguese acronym) performs studies and researches on energy planning. Moreover, in every year, EPE publishes the Ten-Year Energy Expansion Plan (PDE in Portuguese acronym). For the PDE 2030, it is estimated a total of 200,154 km of TL while until August 2020 there were 158,892 km (EPE, 2021).

Concomitantly, it is known that between 80% to 90% of short-circuits on electrical power systems (EPS) happen on TL (TLEIS, 2019). Thus, power systems require quick and selective protection schemes, in order to clear faults and avoid both widespread blackouts and people/equipment damage, as well as accurate fault location algorithms, which are used to speed up the TL restoration after unscheduled shutdowns. Therefore, the Brazilian Transmission

System Operator (ONS in Portuguese acronym) imposes a maximum fault clearance time of 100 ms (ONS, 2021). Aiming to obtain fast and reliable functions, several studies have been reported towards devices capable of performing such protections (SEL-T400L INSTRUCTION MANUAL, 2019; GE, 2009).

It is well known that most TL protection functions are based on fundamental phasors obtained from voltage and current signals measured at the monitored line terminals. Those functions have been successfully applied over the past decades, being embedded in several commercially available devices. At the same time, though, due to the data windowing process to estimate phasors, protection functions available in these devices have inherent delays (PHADKE; THORP, 2009). In addition, fault location methods based on phasor estimation can yield errors between 1% and 5% of the line length, being often dependent on line parameters, which can in turn present uncertainties (ZIMATH *et al.*, 2010). Other problem that can impact in a negative way the phasor based functions are the current transformer (CT) saturation, low fault contribution, among others (SAHA *et al.*, 2009; SCHWEITZER *et al.*, 2016).

Along with the agents needs for fast and reliable TL monitoring, protection techniques have evolved in signal processing aspects, enabling the use of microprocessed relays with sampling frequencies in the order of megahertz. Intelligent electronic devices (IED) using sampling rates from 10 kHz to 1 MHz have allowed the application of time-domain protection algorithms embedded in commercial devices, with average operation time between 1 ms to 5 ms. These high sampling rates have also allowed the extraction of accurate information on traveling waves (TW) launched by faults on TL, what has led TW-based fault location applications to gain popularity over the past years (SEL-T400L INSTRUCTION MANUAL, 2019; SCHWEITZER *et al.*, 2014; RIBEIRO; LOPES, 2018; LOPES *et al.*, 2018). Along with IED advances and time-domain devices available commercially, new studies regarding these solutions become necessary.

1.2 MOTIVATION

Due to the advances in signal processing and A/D converters along with the expectation of achieving high-speed protection and accurate fault location, time-domain functions have attracted an increasing attention from utilities, specially TW-based ones. Consequently, EMTP

softwares have been widely used for tests and validation purposes. Nevertheless, despite the increasing interest from utilities on such a topic, researches focused on the evaluation of impacts of EMTP system models on these time-domain functions are still scarce. Moreover, considering the same perspective, the evaluation of real time-domain relays is also an open topic, which requires clarifications to support reliable laboratory testing procedures.

Commonly, papers apply some line modeling simplifications in relation to the real-world scenario. Despite frequency-dependent lines, transposition schemes and soil heterogeneity along the TL are widely known as TL realistic characteristics (GLOVER *et al.*, 2011; MARTINS-BRITTO, 2020; SIDWALL; FORSYTH, 2020), they are often disregarded. Besides, the impact of combinations of these line modeling approaches are scarcely addressed and there is no consensus whether there are relevant differences in time-domain studies, specially in TW patterns, when different modeling strategies are taken into account.

Aiming to fill the above mentioned knowledge gap, this work performs studies using an EMTP-software, namely, Alternative Transients Program (ATP), considering several modeling scenarios. It also significantly contributes to the scientific community by identifying from comparisons between simulated and real records which line model in ATP is the most representative for real fault scenarios when the TW phenomenon is under investigation. Besides, this work identifies the impact of different TL modeling approaches on TW-and Z-based fault location algorithms, as well as on protection functions embedded in an actual time-domain relay.

1.3 OBJECTIVES

The main goal of this master thesis is to perform massive tests in order to analyze the TL EMTP models influence on the performance of time-domain fault location and protection functions. Therefore, the following specific objectives are defined:

- Identify the line models which induce TW patterns closest to real-world fault scenarios, understanding the most representative features of each EMTP TL models;

- Perform computational assessments about the impact of TL modeling aspects on TW-based fault location (TWFL) algorithms;

- Evaluate the impacts of TL EMTP models on a real time-domain relay, including the evaluation of TW- and Z-based fault location algorithms.

1.4 CONTRIBUTIONS

Along with this work, contributions were presented to the scientific community, showing impacts that some EMTP modeling schemes can pose on time-domain functions. Among these contributions, the following topics stands out:

- Based on simulations, transient propagation patterns are evaluated accounting for amplitude, propagation speed, for both phase and modal signals, being the signals compared with real-world records in order to identify the most realistic modeling approach. Moreover, the effect of different ground resistivities on modal components for TW propagation velocity along the frequency spectrum are investigated;
- Impacts of TL modeling schemes on time-domain protection functions and fault location methods are identified. Also, problems to recognize TW reflected from the fault point in grounded faults are highlighted.

The studies developed during this master thesis resulted in scientific papers related to the research. These papers are listed bellow:

1. L. M. A. Ribeiro, E. P. A. Ribeiro, G. A. Cunha, and F. V. Lopes. Modelagem de Linhas de Transmissão em Programas EMTP: Um Estudo sobre a Propagação de Ondas Viajantes. In: III Simpósio Brasileiro de Sistemas Elétricos 2020, (SBSE 2020). v. 1, n. 1, DOI 10.48011/sbse.v1i1.2449.
2. L. M. A. Ribeiro, G. A. Cunha, E. P. A. Ribeiro, A. G. Martins-Brito, and F. V. Lopes, "Analysis of traveling waves propagation characteristics considering different transmission line emtp models," 5th Workshop on Communication Networks and Power Systems (WCNPS 2020), pp. 1–6.
3. L. Ribeiro, G. Cunha, A. Martins-Britto, E. Ribeiro, and F. Lopes, "Impact of transmission line modeling aspects on tw-based fault location studies" Electric Power Systems Research, vol. 196, p. 107204, 2021.

1.5 THESIS ORGANIZATION

The present work is organized as follows:

- Chapter 2 provides a brief literature review on fault location methods and protection functions.
- Chapter 3 provides theoretical Principles about the topics addresses in this thesis, serving as the basis for the document understanding.
- Chapter 4 describes and explains the investigated protection functions and fault location algorithms.
- Chapter 5 explains the evaluated systems and tests procedures.
- Chapter 6 contains all proposed studies along with their respective obtained results.
- Chapter 7 exposes the thesis conclusions and proposes future works.

CHAPTER 2

LITERATURE REVIEW

Normally, fault location methods are classified as being based on: fundamental components (FC); high frequency components; artificial intelligence; and TW's theory. Fault location methods can also be classified according to other parameters, such as number of monitored terminals, evaluated signals, dependence on aligned time reference, among others (SAHA *et al.*, 2009). FC- and TW-based methods are commonly available in commercially devices, such that, in this work, only these approaches are studied.

In this chapter, relevant publications about TW-based fault location (TWFL) and phasor-based methods are described, including a review on time-domain protection functions embedded in the relays analyzed during this work. Basically, the main concepts of each function are presented, analyzing the operating principles and limitations of the reviewed techniques.

2.1 FUNDAMENTAL COMPONENT-BASED FAULT LOCATION METHODS

This type of method has been extensively applied in commercial devices, being widely reported in the literature. Such a popularity results from their simplicity, which lead these approaches to be easier to implement in the field than other solutions, mainly due to the low sampling rates requirements and small associated computational effort (LOPES, 2014).

In this category, single-ended methods were those that have been firstly developed. Their main advantage consists in its independence of data synchronization and communication channels. Takagi *et al.* (1982) propose a single-ended method that requires pre-fault current and voltage signals, reducing the effect of fault resistance. The key point of Takagi's method is the implementation of incremental-quantities (IQ). Furthermore, it is assumed that fault impedance are completely resistive and that the system is homogeneous. In addition, the method neglects the capacitive effect, since it is based on short TL model. These considerations can

yield additional fault location inaccuracies, especially in long lines.

Salim *et al.* (2011) present an method that considers the TL capacitive effect, overcoming the above-mentioned drawback. However, it still considers the impedance as a pure resistance, similarly to Takagi *et al.* (1982). Over the years, several methods were proposed in order to overcome problems that could arise due to fault resistance effects (DAS *et al.*, 2014). Consequently, methods based in more than one terminal became popular, particularly accounting for two terminal measurement, which are often called double-ended method.

An method based on exact π TL model was proposed by Johns & Jamali (1990), being one of the most referenced methods in the literature. It includes the capacitive effect and propagation parameters in the fault location formulation, depending on the knowledge of series and shunt positive sequence parameters, which in turn may present inaccuracies. The method is possible to be applied in modal and sequence domain, and it requires synchronized measurement data.

Shortly after, Girgis *et al.* (1992) report a new flexible method with the possibility of using two or three terminal, and synchronized or non-synchronized data. However, the proposed method does not consider the line capacitive effect. Likewise (GIRGIS *et al.*, 1992), the method proposed by Tziouvaras *et al.* (2001) can be also applied using data taken from two or three terminals, which can be synchronized or non-synchronized. In this reference, the double-ended is highlighted, being addressed in detail. The method overcomes the pre-fault load flow and mutual coupling between zero-sequence and phases by employing symmetrical component-based solution which analyzes the negative-sequence quantities. On the other hand, the method depends on TL parameters.

Since the early stages of fault location methods, studies are being carried out in order to solve or minimize performance limitations. Hence, several authors have proposed methods with the aim to be independent of line parameters, for instance (RADOJEVIC *et al.*, 2009; HE *et al.*, 2011). However, although they do not need TL parameters, the methods reported in (RADOJEVIC *et al.*, 2009; HE *et al.*, 2011) still depend on data synchronization, which is a characteristic that can also impose practical limitations in the application of such techniques in systems without a common time reference.

The use of non-synchronized data from two terminals or more overcome the need for a common time reference (IZYKOWSKI *et al.*, 2011; SAHA *et al.*, 2013). However, most of these

solutions apply iterative processes in order to calculate synchronization angles between local and remote terminal measurements. Thus, these techniques have become more complex and slower solutions, which limits their online application in power networks.

2.2 TRAVELING WAVE-BASED FAULT LOCATION METHODS

TWFL methods exist since 1931 (BEWLEY, 1931). Nevertheless, the necessity of high sampling rates used to be a limiting factor that raised prices and hampered field implementation initiatives. Therefore, only after recent technological advances, line monitoring devices became able to sample electrical signals with sampling frequencies in the order of megahertz (SCHWEITZER *et al.*, 2014), leading TWFL methods to gain popularity.

In 1993, Gale *et al.* (1993) presented a classical categorization of TWFL methods, which are often divided into different groups. Also, the referred work suggests the use of current signals for TW applications, mainly when one terminal methods are taken into account. Such a recommendation tries to take advantage of the frequency response of current transformers (CT), which are better than those of capacitive voltage transformers (SAHA *et al.*, 2009). Although single terminal methods do not require data synchronization, Gale *et al.* (1993) classify these methods as more complex than double-ended methods, since they need a proper identification of TW reflected from the fault point. Consequently, those techniques that require the detection of only the first incident TW at both line ends are usually refereed as simpler methods, such as the classical two-terminal TWFL method.

Gilany *et al.* (2007) propose a methodology based on two terminal measurements in order to overcome errors due to uncertainties in TW propagation velocity values. This method requires the identification of the first incident TW at both terminals, as well as a the detection of the TW reflected back from the fault point. Despite there is no need to know the TW propagation speed, data synchronization and difficulties to identify reflected TW are limitations of this method. In addition, also trying to eliminate the propagation velocity need from fault location methods, Feng *et al.* (2008) present a three terminal method. However, when considering more then two terminals, the method becomes more complex. Moreover, this technique considers the same propagation velocity on every analyzed line sections, which can become an error source

in the case of using different tower structures in each line.

Lopes (2016) propose a two terminal technique that does not require data synchronization nor TW propagation velocity information. Hence, it is not parameter dependent, which facilitates its application in the field. However, the proposed formulation require the detection of the first incident zero mode TW (TW0), also known as ground mode, at each terminal. Thereby, such an approach is feasible only for grounded faults. Besides, due to the high attenuation from TW0, this method is expected to reliably operate in short TL, presenting additional errors for long lines.

Aiming to overcome the problems reported in the previous paragraph, in 2018 Lopes *et al.* (2018) presented a methodology based on the analysis of aerial mode only. The method needs the identification of the first incident TW and reflect TW in both terminal, being the need of the reflected wave a source of errors. Also, the method considers that the forward and backward waves have the same speed, which pose uncertainties. As the TW detection instants are carried out in an independent way for each terminal, this method does not require data synchronization neither electrical line parameters.

2.3 TIME-DOMAIN PROTECTION FUNCTIONS

Aiming to allow a high speed protection tripping time in transmission line monitoring schemes, time-domain functions have been proposed over the recent years. Here, time-domain protection functions developed by means of IQ or TW quantities are described, emphasizing those embedded in the real TL protection relay evaluated in this work.

Time-domain protection functions overcome the need for phasor estimation, avoiding delays due to data windowing processes (SCHWEITZER *et al.*, 2014). To do so, instantaneous values of monitored quantities are processed, being these signals analyzed over different spectrum ranges. Thereby, it is usually considered that IQ- and TW-based functions analyze instantaneous values of the monitored signals considering lower and upper spectrum bands.

One of the first relays equipped with protection functions based on IQ theory was a directional power relay (CHAMIA; LIBERMAN, 1978). The method helped to improve system stability and power transfer capability. From the polarity difference between incremental vol-

tages and currents, the fault directionality can be determined, i.e., the disturbance is classified as forward or reverse. However, due to the computational limitations from that period, significant delays in signal processing solutions were verified. Concomitantly, the poor transient response of capacitive voltage transformers (CVT) was a problem, jeopardizing the proper fault directionality discrimination (CHAMIA; LIBERMAN, 1978).

In 1981, Vitins (1981) proposes a directional scheme that uses elliptical trajectories described in a plane formed by IQ quantities to identify the fault direction. Aiming to solve problems caused by DC decaying exponential component on current signals, power directional scheme operation time delays were verified, demonstrating the need for restriction region expansion (VITINS, 1981). Thereupon, Lanz *et al.* (1985) show that the elliptical trajectories described in the plane formed by incremental signals were narrowed when replica impedances are used, providing an accurate indication of the fault direction throughout the disturbance duration.

Bewley (1931) allowed great advances in TW theory field, facilitating the understanding of several new TL protection functions. (DOMMEL; MICHELS, 1978) proposed a discriminant factor D, which assumes high values for forward faults, being close to zero for reverse faults. Thereby, from the comparison between the D factor and a threshold, the fault direction can be identified. For this purpose, a low-bandwidth communication channel is required. Besides, CVT with high reliability are needed to obtain information on voltage transients.

Crossley & McLaren (1983) proposed a TW-based distance function which requires one terminal data only. The wave reflected from the fault point is identified using modal components and correlation theory. In this function, firstly, the fault location is estimated and then, the fault location and the protected zone reach are compared, allowing to determine whether the short-circuit is an in- or out-of-zone fault. It is important to highlight that the need for detecting reflected waves is considered a challenging task, being reported as a limitation of one-terminal methods.

Takagi *et al.* (1977) and Takagi *et al.* (1979) proposed TL differential functions based on TW analysis. The method applies Bergeron equations to analyze voltage and current incident waves in order to obtained differential signals. It was concluded that for in-zone faults scenarios, the differential-quantity is expected to increase, whereas it becomes close to zero for out-of-zone faults, making feasible the accurate in-zone fault identification. However, due to the voltage

analysis, highly reliable CVT are required to assure dependable tripping commands.

Other distance function based on IQ quantities is presented by Dzienis *et al.* (2010). Operation and restriction voltages in the protection zone range are estimated by pre-fault voltage and current measurements as well as voltage and current IQ signals. Tests in real devices were performed and it was concluded that the DC decaying exponential component delays the protection operation time. In addition, aiming to reduce the effects of high frequency components on the method, operation quantity average values are computed, being considered in the relay tripping logic. Consequently, the average relay operation time is of about 12 ms (DZIENIS *et al.*, 2010)

In order to improve the CVT frequency response, obtaining faster operation time and a more robust and secure method, Finney *et al.* (2010) propose a distance element which uses Clarke's transformation together with a filter to analyze power system signals. In addition, Schweitzer *et al.* (2014) propose different TL protection functions applied in time-domain based on IQ and TW theory. In this context, some functions stand out, namely: TD21, TD32, TW32 and TW87. TD21 is a distance function based on IQ; TD32 and TW32 are directional functions based on IQ and TW theory, respectively, which use a POTT (Permissive Overreaching Transfer Trip) scheme; and TW87 is a differential function based on TW.

Functions based in IQ processing uses incremental replica current to eliminate DC decaying component from current signals, allowing the analysis of the monitored system as a resistive circuit. By doing so, greater security is guaranteed for the available IQ-based functions, facilitating the calculation of settings as well. In addition, the TD21 function is implemented by rules that verified the behavior of line voltage profile, specifically at the protected zone reach point. As a result, faults within the protection zone can be detected whenever the voltage variation at the protected zone reaching point exceeds the pre-fault voltage at the same location. For ultra-high-speed operation, TW32 is used, requiring to identify the first incident TW voltage and current polarities. Moreover, the TW87 needs only current TW (SEL-T400L INSTRUCTION MANUAL, 2019), although it requires some supervision elements which depend on voltage measurements. Schweitzer *et al.* (2016) demonstrated that these protection functions operated faster than traditional methods and, since these publications, these time-domain functions have been increasingly used in real power networks.

2.4 LITERATURE REVIEW SUMMARY

With the aim to better emphasize the characteristics of the evaluated literature, Tables 2.1 and 2.2 are presented containing a summary of the main characteristics evaluated. In each table, details on the studied works are highlighted.

In this work, in order to provide a comprehensive analysis, FC- and TW-based fault location methods as well as the protection functions reported in (SCHWEITZER *et al.*, 2014) are evaluated, which some of them are available in a real time-domain protective relay, as it will be explained in the next sections.

Table 2.1. Bibliographic review summary of fault location methods

Reference	Method classification	Numbers of terminals required	TL parameters need?
Takagi *et al.* (1982)	FC	1	✓
Salim *et al.* (2011)	FC	1	✓
Johns & Jamali (1990)	FC	2	✓
Girgis *et al.* (1992)	FC	2	✓
Radojevic *et al.* (2009)	FC	2	×
He *et al.* (2011)	FC	2	×
Tziouvaras *et al.* (2001)	FC	2	✓
Izykowski *et al.* (2011)	FC	2	✓
Saha *et al.* (2013)	FC	2	✓
Gale *et al.* (1993)	TW	1 and 2	✓
Gilany *et al.* (2007)	TW	2	×
Feng *et al.* (2008)	TW	3	×
Lopes (2016)	TW	2	×
Lopes *et al.* (2018)	TW	2	×

Table 2.2. Bibliographic review summary of time-domain TL protection functions

Reference	32	21	87
Chamia & Liberman (1978)	✓	×	×
Vitins (1981)	✓	×	×
Lanz *et al.* (1985)	✓	×	×
Dommel & Michels (1978)	✓	×	×
Crossley & McLaren (1983)	×	✓	×
Takagi *et al.* (1977), Takagi *et al.* (1979)	×	×	✓
Dzienis *et al.* (2010)	×	✓	×
Finney *et al.* (2010)	×	✓	×
Schweitzer *et al.* (2014)	✓	✓	✓

CHAPTER 3

THEORETICAL PRINCIPLES

In this chapter, the theoretical principles of time-domain fault location and protection functions are presented, considering TW- and IQ-based approaches. This chapter is fundamental to understand the results that will be discussed in the next chapters of this thesis. In sequence, the next chapter describes the analyzed functions accounting for relay procedures and computational tests.

3.1 THEORY OF TRAVELING WAVES

When faults take place on TL, an abrupt voltage variation is verified, modifying the system normal operation point. As a consequence, electromagnetic transients are induced, which propagate from the fault point towards both line ends. These electromagnetic transients are referred as voltage and current TW. In overhead TL, these TW propagate with velocities very close to the speed of light (BEWLEY, 1931; PHADKE; THORP, 2009), being of about $c = 299{,}792.458$ km/s.

By means of a pure fault circuit, such as illustrated in Figure 3.1, the TW phenomenon can be explained, assuming that an abrupt voltage variation occurs in the voltage profile at the fault point. In Figure 3.1, V_f is the instantaneous voltage value at the fault point immediately before the disturbance takes place, which can be obtained as a function of the system voltage as $V_f = V_{\text{syst}} \cdot \sin\theta$, in which θ is the fault inception angle. Still in Figure 3.1, Rf is the fault resistance, V_{TW} and I_{TW} represent the voltage and current TW amplitudes, respectively, and Z_S represents the TL surge impedance (RIBEIRO *et al.*, 2018; LOPES *et al.*, 2019a; SCHWEITZER *et al.*, 2014). It is important to highlight that, as the line terminations do not impact on the amplitudes of TW launched at the fault point, the terminations are not illustrated in the figure (SCHWEITZER *et al.*, 2014).

Considering that TW are generated by step changes in voltage profile on the line, associated transients can take place at different spectrum parts, being predominantly analyzed in high frequency spectrum ranges. Thereby, since in high frequencies reactance and susceptance values are much greater than resistance and conductance ones, a common simplification consists in disregarding TL losses (ARAUJO; NEVES,). Hence, the surge impedance can be considered during the analysis of TW, without loss of reliability, as shown in (3.1), in which L is the line inductance and C, the capacitance.

$$Z_S = \sqrt{\frac{\mathrm{j}\omega L}{\mathrm{j}\omega C}} = \sqrt{\frac{L}{C}} \ . \tag{3.1}$$

V_{TW} is obtained from the Kirchhoff's Law applied to the circuit illustrated by Figure 3.1. For a single-phase fault, V_{TW} and I_{TW} are calculated according to (3.2) and (3.3), respectively, being Z_{S0} the ground mode surge impedance and Z_{S1} the aerial mode surge impedance (PHADKE; THORP, 2009).

$$V_{\mathrm{TW}} = -V_f - 2 \cdot R_f \cdot I_{\mathrm{TW}} = -V_{\mathrm{Sys}} \cdot \sin(\theta) - 2 \cdot R_f \cdot I_{\mathrm{TW}} \ , \tag{3.2}$$

$$I_{\mathrm{TW}} = \frac{-3 \cdot V_f}{Z_{S0} + 2 \cdot Z_{S1} + 6 \cdot R_f} \ . \tag{3.3}$$

From the presented equations, it can be concluded that for high values of R_f and $\theta \approx 0°$ or $\theta \approx 180°$ (under a sinusoidal reference) no voltage step change is verified, since they coincide with instants at which the system voltage crosses zero. Also, step changes in voltage and current signals are observed as soon as the firsts TW reach the line terminal, getting attenuated as the signals propagate (LOPES *et al.*, 2019a).

Figure 3.1. Pure fault circuit.

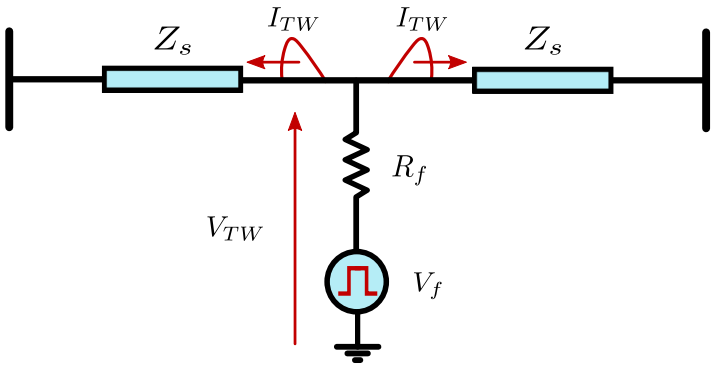

Source: adapted from Lopes *et al.* (2019a).

3.2 TRAVELING WAVE DETECTION

Several TW detection techniques have been reported in literature in order to extract TW amplitude and polarity information. Among these methodologies, some stand out, namely: Discrete Wavelet Transform (DWT) and Maximal Overlapped Discrete Wavelet Transform (MODWT) (SAHA *et al.*, 2009; COSTA *et al.*, 2011; PERCIVAL; WALDEN, 2000); Park's Transformation (TDQ) (LOPES *et al.*, 2013); Finite Impulse Response (FIR) filters (ZIMATH *et al.*, 2010); and Differentiator-Smoother (DS) filter (SCHWEITZER *et al.*, 2014).

In several applications, the DS filter has been highlighted for maintaining an unitary gain and for allowing an easy evaluation of TW polarities. This filter is embedded in commercially devices equipped with TW-based fault location and protection applications (SCHWEITZER *et al.*, 2014; SCHWEITZER *et al.*, 2016), such as the one analyzed in this work. The filter creates patterns on its outputs, converting fault induced step changes into triangular-shaped outputs, through which the TW arrival time can be detected at the monitored terminal (SCHWEITZER *et al.*, 2016). Hence, further details on the DS filter are presented next.

3.2.1 The DS Filter

This filter consists in a two stage implementation. Firstly, the transient signal is smoothed and then, in the second stage, the signal is differentiated. The smoother stage is a low-pass filter that reduces the effects of waveform distortions over the step change of interest. On the other hand, as mentioned earlier, the second stage transform the step-like transients into a triangular pulse-like shaped signal (SCHWEITZER *et al.*, 2014). For attenuated transients, the input signal gets a ramp format, leading the DS filter output to be a parabola-shaped waveform (LOPES *et al.*, 2019a), as depicted in Figure 3.2.

The DS filter used in the evaluated device applies N_{DS} coefficients, having half less one of the filter coefficients set with positive gain G, and the remaining ones with $-G$ values. A central null coefficient is taken into account, resulting in $N_{\mathrm{DS}} = 21$ coefficients. In order to obtain the unitary gain, the gain G must be equal to $G = \frac{2}{N_{\mathrm{DS}}-1}$ (RIBEIRO *et al.*, 2019).

Figure 3.2. DS filter response.

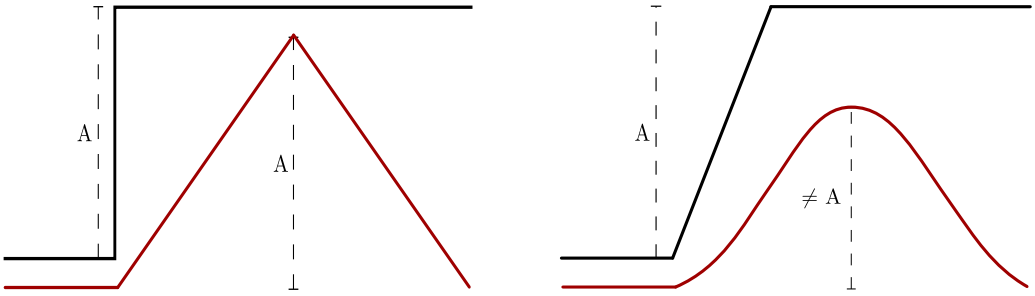

Source: own authorship.

3.2.2 Bewley Diagram

Bewley (1931) proposes a diagram which aims to facilitate the understanding of the TW propagation phenomenon on TL. Known as Bewley diagram, it depicts the TW propagation patterns over the space and time, allowing to analyze TW arrival times and the traveled line portions. Being the TW propagation velocity dependent on TL parameters ($v_{\mathrm{pTW}} = \sqrt{\frac{1}{LC}}$) (Greenwood, 1971), lattices are formed with angles which are proportional to v_{pTW}, leading this diagram to be widely known as lattice diagram as well. Besides, the propagation time (τ) is the time that a TW takes to propagate from one TL terminal to another, being defined as $\tau = l/v_{\mathrm{pTW}}$, in which l is the line length.

The Bewley diagram of fault-induced TW on an overhead TL is represented in Figure 3.3, where d is the fault distance from the local terminal (Bus 1). The monitored TL connects local

Figure 3.3. Bewley Diagram.

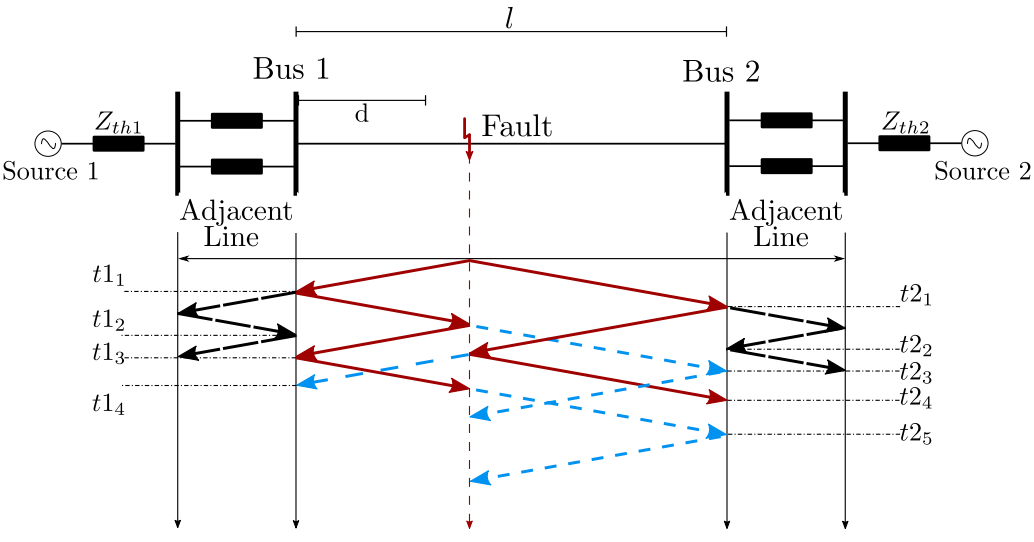

Source: own authorship.

and remote terminals, and it includes adjacent lines between the monitored TL and system sources. Moreover, the diagram illustrates incident, reflected and refracted TW, allowing the analysis of their respective arrival instants at each terminal.

TWFL techniques require the proper identification of incident, reflected or refracted time-stamps. For instance, in Figure 3.3, $t1_1$ is the instant at which the incident TW reaches Bus 1, while $t1_3$ is the instant at which the TW reflected from the fault point arrives at Bus 1. Therefore, for the correct functioning of TWFL methods, the Bewley diagram analysis is quite useful, which justifies its explanation in this section.

3.2.3 Clarke's Transformation

The Clarke's transformation has been successfully applied in real TW-based devices in order to decouple three-phase systems and represent the signals in modal-domain accounting for aerial (alpha and beta) and ground (zero) modes (CLARKE, 1943; SCHWEITZER *et al.*, 2014). Here the ground mode is represented as TW0, the alpha, as TW1 and beta, as TW2, being TW0 only expected to exist in grounded faults. In addition, in single-phase faults cases, TW2 is not expected to exist, while for double-phase faults it is considered the reference mode to be analyzed. The transformation can be referred to phases A, B or C, as shown next in (3.4), (3.5) and (3.6), respectively (SCHWEITZER *et al.*, 2014):

$$\begin{bmatrix} TW1_{\mathrm{a}} \\ TW2_{\mathrm{a}} \\ TW0_{\mathrm{a}} \end{bmatrix} = \frac{1}{3} \cdot \begin{bmatrix} 2 & -1 & -1 \\ 0 & \sqrt{3} & -\sqrt{3} \\ 1 & 1 & 1 \end{bmatrix} \cdot \begin{bmatrix} TW_{\mathrm{A}} \\ TW_{\mathrm{B}} \\ TW_{\mathrm{C}} \end{bmatrix} , \tag{3.4}$$

$$\begin{bmatrix} TW1_{\mathrm{b}} \\ TW2_{\mathrm{b}} \\ TW0_{\mathrm{b}} \end{bmatrix} = \frac{1}{3} \cdot \begin{bmatrix} -1 & 2 & -1 \\ -\sqrt{3} & 0 & \sqrt{3} \\ 1 & 1 & 1 \end{bmatrix} \cdot \begin{bmatrix} TW_{\mathrm{A}} \\ TW_{\mathrm{B}} \\ TW_{\mathrm{C}} \end{bmatrix} , \tag{3.5}$$

$$\begin{bmatrix} TW1_{\mathrm{c}} \\ TW2_{\mathrm{c}} \\ TW0_{\mathrm{c}} \end{bmatrix} = \frac{1}{3} \cdot \begin{bmatrix} -1 & -1 & 2 \\ \sqrt{3} & -\sqrt{3} & 0 \\ 1 & 1 & 1 \end{bmatrix} \cdot \begin{bmatrix} TW_{\mathrm{A}} \\ TW_{\mathrm{B}} \\ TW_{\mathrm{C}} \end{bmatrix} , \tag{3.6}$$

in which TW_{A}, TW_{B} and TW_{C} are the input phase signals (voltage or current). Thereby, depending on the fault type, the correct matrix must be selected, allowing to take into consideration the transient quantities which are indeed excited by the fault.

3.3 INCREMENTAL-QUANTITY DETECTION TECHNIQUES

Voltage or current at any power grid point can be calculated as the algebraic sum of individual system sources contributions according to the superposition theorem (IRWIN; NELMS, 2010). Consequently, it is possible to separately model an electric system under fault conditions as the electric grid contribution, namely, pre-fault circuit, and the fault contribution, known as pure fault circuit. The pre-fault circuit represents the load signals during the system normal operation, while the pure fault circuit presents uniquely the variations in the signals generated by the short-circuit. Hence, during a fault, voltage and current at any electrical grid point are obtained by pre- and pure fault contributions superposition.

Knowing the electrical quantities at the TL terminals before and after the fault, and subtracting the pre-fault contributions from the measurements taken during the fault period, it is possible to estimate the contribution generated exclusively by the fault, i.e., the pure fault circuit quantities. The signals obtained by such calculation is traditionally known as IQ, being mathematically obtained as follows (SCHWEITZER *et al.*, 2014):

$$\Delta s(t) = s(t) - s(t - p \cdot T) \ , \tag{3.7}$$

in which $\Delta s(t)$ is the instantaneous IQ, $s(t)$ is the instantaneous measured current or voltage signal, T is the signal fundamental period whereupon the IQ is obtained, and p is an arbitrary number of cycles that determines the duration of the resulting IQ. Figure 3.4 illustrates the current IQ obtained from different p values. In this way, ideally, the IQs contain information about the fault transients at any spectrum range (RIBEIRO, 2019).

Figure 3.4. Current signals: (a) Load current; (b) Monitored current; (c) Current IQ obtained from different p values.

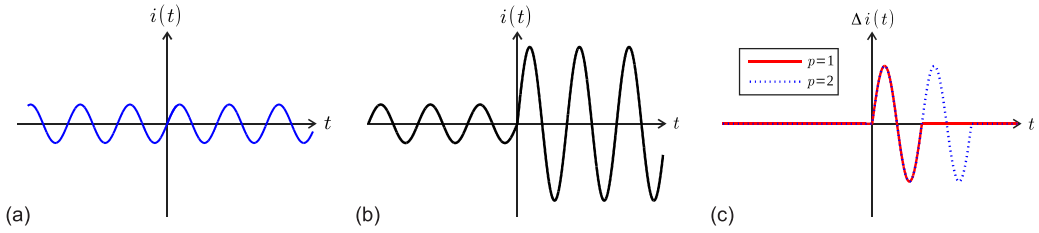

Source: (RIBEIRO, 2019).

It is noticed from (3.7) that the IQ has a time period proportional to $p \cdot T$ during which it is valid in practical applications. Hence, after this period, the obtained signals from the

equation can not be used, once all samples are on fault period, losing the samples related to the pre-fault state. Hence, IQ-based protection functions should be blocked p cycles after the fault beginning (SCHWEITZER *et al.*, 2016; SEL-T400L INSTRUCTION MANUAL, 2019), otherwise, unreliable operations can take place.

The protective relay tested in this work requires instantaneous signal samples to analyze their magnitudes and polarities. Thus, although system loading effects are reduced in pure fault circuit (being ideally nonexistent), Δs may still presents angle displacements due to the inductive effects of the line, making difficult the to compare signals in time-domain (LOPES *et al.*, 2020). Therefore, replica currents are also calculated in the time-domain evaluated relay, aligning voltage and replica currents, such that the monitored circuit can be evaluated such as if it were a resistive circuit. By doing so, polarity and amplitude comparisons become more reliable and easier to carry out.

CHAPTER 4

ANALYZED PROTECTION AND FAULT LOCATION FUNCTIONS

4.1 PROTECTION FUNCTIONS

The time-domain protection functions analyzed in this work are described in this chapter. The main features of each function are presented, detailing information needed to understand the performed tests and studies.

4.1.1 Time-Domain Distance Element - TD21

TD21 is an underreach distance protection function which needs only one terminal data to issue trip commands. Thus, it can be applied in a stand alone protection scheme, in which communication channels are not needed. Moreover, this function uses a Direct Transfer Trip (DTT) pilot protection scheme (SEL-T400L INSTRUCTION MANUAL, 2019), speeding up the fault clearance when out-of-zone faults take place in relation to one of the line terminals.

The operation principle of the TD21 function is based on the TL voltage profile. Basically, restraining ($V_{21\mathrm{R}}$) and operating voltages ($V_{21\mathrm{OP}}$) are estimated at the protection reaching point, being compared between themselves. Therefore, when the operation voltage is greater than the restriction voltage, i.e., $V_{21\mathrm{OP}} \geq V_{21\mathrm{R}}$, the fault is identified as an in-zone fault (SCHWEITZER *et al.*, 2016), otherwise, an out-of-zone is declared.

To properly understand the TD21 operation, it is worthy to know how $V_{21\mathrm{OP}}$ and $V_{21\mathrm{R}}$ are calculated. As a first step, the pre-fault voltage (V_f) evaluation at the protection reaching point m_0 is calculated using:

$$V_f = V - m_0 \cdot |Z_{\mathrm{TL}}| \cdot I_z \ , \tag{4.1}$$

whereupon Z_{TL} is the absolute value of the positive-sequence line impedance, V is the measured

voltage and I_z is the non-incremental replica current obtained from measured currents.

$V_{21\mathrm{OP}}$ is calculated from the pure fault circuit and it represents the voltage variation at the protection reaching point when a fault occurs. Thereby, V_{21OP} is defined as follows:

$$V_{21\mathrm{OP}}(t) = V_f(t) - V_f(t-T) = \Delta v - m_0 \cdot |Z_{\mathrm{TL}}| \cdot \Delta I_z \ . \tag{4.2}$$

As solid faults consist in the most adverse scenarios from the point of view of voltage sags, the TD21 considers $V_{21\mathrm{R}}$ as being the pre-fault voltage at the reaching point, which can be calculated by using samples taken from the steady-state system regime, typically obtained one fundamental cycle before the disturbance detection instant. Hence, $V_{21\mathrm{R}}$ can be expressed as:

$$V_{21\mathrm{R}}(t) = V_f(t-T) \ . \tag{4.3}$$

The TD21 scheme also considers a directional overcurrent element (OC21) and the directional time-domain element TD32, which supervise the distance protection operation. By doing so, the TD21 security increases, avoiding false trips during low energy non-fault events (SCHWEITZER *et al.*, 2016; SEL-T400L INSTRUCTION MANUAL, 2019; LOPES *et al.*, 2020).

4.1.2 Time-Domain Directional Element - TD32

The TD32 function is an IQ-based directional function able to operate in few milliseconds by identifying the fault direction. It is worthy to notice that the TD32 does not trip alone, requiring the application of a pilot scheme. In the evaluated time-domain protective device, a POTT scheme is applied (SEL-T400L INSTRUCTION MANUAL, 2019), whose operation principle is based on the comparison between the detected fault direction at both line terminals.

In summary, the TD32 analyzes incremental voltages and incremental replica currents, comparing their polarities in order to discriminate the fault direction (SCHWEITZER *et al.*, 2016; SEL-T400L INSTRUCTION MANUAL, 2019). To do so, it calculates an operating torque (T_{OP}), which is given by the negative value of the product between incremental voltage (ΔV) and replica current (ΔI_z), as follows:

$$T_{\mathrm{OP}}(t) = -\Delta V \cdot \Delta I_z \ . \tag{4.4}$$

In reverse fault cases, ΔV and ΔI_z present the same polarity, resulting in $T_{\mathrm{OP}} < 0$. On the other hand, in forward fault cases, ΔV and ΔI_z present opposite polarity, yielding $T_{\mathrm{OP}} \geq 0$ (SEL-T400L INSTRUCTION MANUAL, 2019). In this context, it important to point out that, since the replica current calculation does not completely eliminate the inductive line characteristic effect, T_{OP} can result in uncertainties regarding the fault direction when ΔV and ΔI_z present low values. Therefore, a security margin (SM) is considered in the TD32 algorithm.

4.1.3 Traveling Wave Directional Element - TW32

This function compares the voltage (V_{TW}) and current (I_{TW}) incident TWs polarities defining the fault direction in relation to the monitored terminal (SEL-T400L INSTRUCTION MANUAL, 2019). In reverse faults, V_{TW} and I_{TW} present the same polarity at the closest monitored terminal from the fault point, but present opposite polarities at the opposite terminal through which they leave the line. These signals are extracted by means of the DS filter, being used to calculate an operation torque, which is given by:

$$T_{\mathrm{OP}} = -V_{\mathrm{TW}} \cdot I_{\mathrm{TW}} \ . \tag{4.5}$$

Since the TW32 operates based on the first incident fault-launched waves, its operation time generally occurs up to a few hundred microseconds after the fault inception. However, such a function does not trip the line alone, requiring the POTT scheme operating in conjunction with the TD32 function to yield trip commands to the associated circuit breakers (SCHWEITZER *et al.*, 2016; SEL-T400L INSTRUCTION MANUAL, 2019). Finally, similarly to the TD21 function, both TD32 and TW32 count on an overcurrent supervision (OCTP), which guarantees that the POTT scheme operates only for fault cases. In this sense, the TD32 starts the fault detection process, being the TW32 element only responsible to accelerate the POTT operation.

4.1.4 Traveling Wave Differential Element - TW87

The TW87 is a differential TL element that requires only the first incident current TWs in both terminals to identify whether the fault is external or internal to the protected line. Using a communication channel to guarantee the two-terminal synchronization and to exchange

information between local and remote terminals, it is possible to compare magnitude and polarity of incident and exit TWs, allowing the discrimination between internal and external fault events (SCHWEITZER *et al.*, 2016; SEL-T400L INSTRUCTION MANUAL, 2019).

The TW87 function is based on the comparison between operating and restraining waves, which are called I_{OP} and I_{RT}, respectively. Basically, I_{OP} is calculated as follows:

$$I_{\mathrm{OP}} = |I_{\mathrm{TWL}}(t \pm P) + I_{\mathrm{TWR}}(t)| \ , \tag{4.6}$$

in which I_{TWL} and I_{TWR} are the amplitudes of incident current TWs that reach local and remote terminals, respectively, and P is the time difference between current TWs arrival time at both ends, being $P < \tau$ for internal faults and $P \approx \tau$ for external faults, being τ the line travel time.

The TW87 considers two restraining variables, namely: I_{RTL} and I_{RTR} for local and remote buses, respectively. Once TWs that leave the line have opposite polarities in relation to those that enter the protected line, I_{RTL} and I_{RTR} can be obtained as follows:

$$I_{\mathrm{RTL}} = |I_{\mathrm{TWL}}(t \pm \tau) - I_{\mathrm{TWR}}(t)| \ , \tag{4.7}$$

$$I_{\mathrm{RTR}} = |I_{\mathrm{TWR}}(t \pm \tau) - I_{\mathrm{TWL}}(t)| \ , \tag{4.8}$$

which are used to calculate:

$$I_{\mathrm{RT}} = \max(I_{\mathrm{RTL}}, I_{\mathrm{RTR}}) \ , \tag{4.9}$$

such that the TW87 identifies an internal fault when $|I_{\mathrm{OP}}| > S \cdot I_{\mathrm{RT}}$, being S a restraining factor (SEL-T400L INSTRUCTION MANUAL, 2019). This function also counts on an overcurrent supervision (OC87), which is based on the analysis of IQ currents, and also on a double-ended fault location element, so that tripping commands are issued only if faults within the monitored line are identified.

4.2 FAULT LOCATION ALGORITHMS

Various fault location algorithms are assessed in this work. Here, TW- and impedance (Z)-based methods are taken into account, considering: the Classical One-Terminal method (C1T) (GALE *et al.*, 1993), Classical Two-Terminal method (C2T) (GALE *et al.*, 1993), Settings-Free Two-Terminal method (GIL) (GILANY *et al.*, 2007) and Settings-Free Two-Terminal Asynchronous method (FLO) (LOPES *et al.*, 2018). These TW-based fault location (TWFL) techniques

present different characteristics, being all based on aerial mode decoupled quantities obtained from the Clarke's transformation.

The relay used in this work have four embedded fault location methods, namely: Single-ended TW-based fault location method (SETWFL); Double-ended TW-based fault location method (DETWFL); Single-ended Z-based fault location method (SEZFL); and Double-ended Z-based fault location method (DEZFL) (SEL-T400L INSTRUCTION MANUAL, 2019). It is noteworthy to highlight that SETWFL and DETWFL can be obtained through the same formulation as C1T and C2T methods, respectively. Thereby, although the analyzed relay applies particular solutions, SETWFL and DETWFL will be referred to as C1T and C2T, respectively.

4.2.1 Classical One-Terminal TWFL Method - C1T

As explained in the bibliographic review, one-terminal TWFL methods require the detection of reflected TWs from the fault point to pinpoint the fault, what can pose difficulties for practical applications. Besides the reflected TW identification, the method requires the TW propagation speed v_{pTW} or the TW propagation time τ to be set. Using the Bewley diagram presented in Figure 3.3, it is possible to calculate the fault distance d in kilometers from the local bus, as follows (GALE *et al.*, 1993):

$$d_{\mathrm{C1T}} = 0.5 \cdot (t1_3 - t1_1) \cdot v_{\mathrm{pTW}} \ , \tag{4.10}$$

in which $t1_3$ is the arrival time of the TW reflected from fault point that reaches Bus 1, and $t1_1$ is the arrival time of the first incident TW at the local terminal. Furthermore, since it depends on v_{pTW} or τ, the formulation is susceptible to errors due to the uncertainties in these variables.

It should be noticed that the reflected wave may be superimposed or mixed with other TWs coming from adjacent TLs or from the remote terminal, making it difficult to identify. Thus, this problem is often reported as one of the biggest challenges to apply this method. Furthermore, for faults involving ground, the mixing mode phenomenon occurs, leading different modes to interact, creating reflections and refractions at the monitored terminal which are not related to the expected patterns for the aerial mode TWs launched by the analyzed fault (PHADKE; THORP, 2009; MAGALHAESJR; LOPES, 2021). Such phenomenon is also

considered a challenge for the reflected wave recognition.

4.2.2 Classical Two-Terminal TWFL Method - C2T

Similarly to the C1T method, the C2T formulation reported by Gale *et al.* (1993) also requires v_{pTW} or τ to calculate the fault location. In addition, the length l and the first incident wave detection at both line ends are required. It is particularly important for this method to guarantee that local and remote data are synchronized. Thereby, since the channel latency variability can interfere or the time alignment signals can be lost, synchronization deviations can take place, resulting in additional fault location errors.

Along with the Figure 3.3, the fault distance d_{C2T} in kilometers can be obtained using (4.11), in which $t2_1$ is the incident TW arrival time at Bus 2 and $t1_1$ at Bus 1.

$$d_{\mathrm{C2T}} = 0.5 \cdot [l - (t2_1 - t1_1) \cdot v_{\mathrm{pTW}}] \ . \tag{4.11}$$

4.2.3 Settings-Free Two-Terminal TWFL Method - GIL

Gilany *et al.* (2007) propose a method that require the first incident TW detection at both line ends, but adding the detection of reflected TWs at one terminal to eliminate the need for propagation velocity settings. Hence, the GIL algorithm is segregated into two formulations, being applied for faults within the first line half section or on the second half section. The fault distance d_{GIL} is calculated as follows:

$$d_{\mathrm{GIL}} = l \cdot \frac{0.5}{1 + \frac{t2_1 - t1_1}{t1_3 - t1_1}} \ , \tag{4.12}$$

$$d_{\mathrm{GIL}} = l \cdot \left(1 - \frac{0.5}{1 + \frac{t1_1 - t2_1}{t1_4 - t1_1}} \right) \ , \tag{4.13}$$

in which (4.12) and (4.13) are applied for faults within the first and second line halves, respectively. According to Figure 3.3, $t2_1$ and $t1_1$ are the first incident TWs at remote and local terminal, respectively, while $t1_3$ is the first reflected TW from the fault point at local bus and $t1_4$ is the refracted TW through the fault point at Bus 1.

4.2.4 Settings-Free Two-Terminal Asynchronous Method - FLO

The FLO method proposed by Lopes *et al.* (2018) does not require data synchronization nor TL parameters to be set, which is considered a huge advantage in the context of practical applications. It depends only on the difference between the time-stamp from the first incident TW and those reflected from the fault point at both terminals, which is, as explained earlier, the main challenge of this method. Based on that, the fault distance d_{FLO} in kilometers can be calculated using:

$$d_{\mathrm{FLO}} = \frac{t1_3 - t1_1}{(t1_3 - t1_1) + (t2_4 - t2_1)} \cdot l \ , \tag{4.14}$$

whereupon $t1_1$ and $t2_1$ are the arrival instants of the first incident TW at local and remote terminals, respectively, being $t1_3$ and $t2_4$ the arrival instants of the TWs reflected from the fault point that reach local and remote terminals, respectively.

4.2.5 Single-ended Z-based Fault Location Method - SEZFL

This algorithm uses the negative-sequence current polarization for unbalanced faults and incremental positive-sequence polarization for three-phase symmetrical faults. The method depends on the selection of the fault loop quantities. After selecting the correct faulted loop, voltage and current phasors for the selected loop are calculated, which are called here $\widehat{V}_{\mathrm{LP}}$ and $\widehat{I}_{\mathrm{LP}}$, respectively. Then, the polarizing current is obtained I_{POL} (SEL-T400L INSTRUCTION MANUAL, 2019). Therefore, the fault distance d_{SEZ} can be calculated, in kilometers, according to the following formulation:

$$d_{\mathrm{SEZ}} = l \cdot \frac{\mathrm{Im}(\widehat{V}_{\mathrm{LP}} \cdot \widehat{I}^{*}_{\mathrm{POL}})}{\mathrm{Im}(Z_1 \cdot \widehat{I}_{\mathrm{LP}} \cdot \widehat{I}^{*}_{\mathrm{POL}})} \ , \tag{4.15}$$

in which Z_1 is the TL positive-sequence impedance, Im stands for the imaginary part of a complex number and $\widehat{I}^{*}_{\mathrm{POL}}$ is the complex conjugate of $\widehat{I}_{\mathrm{POL}}$.

4.2.6 Double-ended Z-based Fault Location Method - DEZFL

The DEZFL method is based on negative-sequence voltage profile along the line during the fault. The algorithm uses local and remote voltage and current phasors to obtain the fault

distance, considering a short line model (SEL-T400L INSTRUCTION MANUAL, 2019). In summary, the algorithm assumes that the voltage at the fault point can be obtained by means of measurements taken from both terminals, so that it can be eliminated from the fault location formula. Hence, the fault distance d_{DEZ} is calculated in kilometers as follows:

$$d_{\mathrm{DEZ}} = l \cdot \mathrm{Re}\left[\frac{(\widehat{V}_{2\mathrm{L}} - \widehat{V}_{2\mathrm{R}}) + Z_1 \cdot \widehat{I}_{2\mathrm{R}}}{Z_1 \cdot (\widehat{I}_{2\mathrm{L}} + \widehat{I}_{2\mathrm{R}})}\right] , \tag{4.16}$$

where $\widehat{V}_{2\mathrm{L}}$ and $\widehat{I}_{2\mathrm{L}}$ are the negative-sequence voltage and current measurements taken from the local terminal, and $\widehat{V}_{2\mathrm{R}}$ and $\widehat{I}_{2\mathrm{R}}$ the measurements obtained from the remote terminal (SEL-T400L INSTRUCTION MANUAL, 2019).

CHAPTER 5

METHODOLOGY

In this chapter, the evaluated systems with their respective characteristics are presented along with the methodology applied in the studies, which were in turn carried out with the aim to assess the impact of different line modeling schemes on time-domain functions. Therefore, EMTP computational simulations and experimental procedures are taken into account.

5.1 TESTING PROCEDURES

The procedures performed for to assess the modeled TL considering different protection and fault location methods can be understood by two stages. The first is related to computational simulations, while the second stage concerns to experimental evaluations with a commercial relay. As it is intended to evaluate only the transients propagation patterns and, mainly, the performance of protection and fault location functions, only solid faults are taken into account to enable the desired evaluation without the influence of the fault impedance on the signal. Besides, the fault initiates at the voltage peak at the fault point.

5.1.1 Computational Simulations

This procedure consists in the implementation of the TW detection technique based on the DS filter followed by transient analysis and TW-based fault location method implementation in programming interfaces. The transient propagation patterns are studied using the case study system illustrated in Figure 5.2, while the fault location methods are applied in signals obtained from fault simulations at the system modeled in Figure 5.4.

The signal acquisition is carried out by massive fault simulations in ATP software and the DS filter is applied in all signals to allow the evaluation of TW amplitudes and arrival times, which

are associated to the time-stamp at the peak of the DS filter triangular/parabolic output. It is worthy to emphasize that, in these studies, the Clarke's transformation was applied to separate the aerial mode quantities from ground mode signals.

For the evaluation of TWFL methods performance according to the TL modeling characteristics, four different methods are implemented in order to investigate their respective impacts on TWFL solutions, considering methods that require only the first incident TW detection or the detection of incident and fault-reflected TW. Methods dependent and independent on information about TW propagation speed or time are also assessed, thereby, requiring the knowledge of TL electrical parameters. This consideration is also relevant due to possible errors that may arise due the frequency-dependence or environmental features variation along the right-of-way. As some methods require the propagation speed, it is obtained by line energization maneuvers simulated at ATP. The obtained speed is shown at Table 5.1 along with the percentages in relation to the speed of light ($c = 299792458$ m/s).

Table 5.1. Power Systems Propagation Speeds

System	Propagation speed (m/s)	Compared to c
1 to 4	290286243.06	96.83%
5 and 7	295574120.60	98.59%
6	295759899.43	98.66%
8	295945911.95	98.72%

The four TWFL methods analyzed in this work are called: C1T; C2T; FLO; and GIL. Their respective formulations have already been explained in the previous chapter. In addition, the methodology implemented to obtain the reflected wave from the fault point is reported in (Guzmán *et al.*, 2018) and (III SCHWEITZER *et al.*, 2019). Basically, the method identifies the polarity of the first incident TW on the analyzed terminal and hypotheses on the TW reflected from the fault are created within a pre-defined observation window. For each hypothesis, weights are calculated, being the hypothesis with the highest weight the estimated response of the function for the arrival time of interest, i.e., the time instant at which the TW reflected from the fault point reaches the monitored terminal. After the fault location is obtained for each method, their respective absolute errors are evaluated.

5.1.2 Relay Testing Methodology

ATP and the analyzed time-domain relay from Schweitzer Engineering Laboratories (SEL) do not have promptly available solutions for massive simulations. Therefore, the Protection Laboratory (LAPSE) in the University of Brasilia (UnB) developed a laboratory test tool in order to allow massive simulations using the time-domain SEL-T400L relay. The complete testing methodology diagram is depicted in Figure 5.1.

As shown in Figure 5.1, from the model file generated by ATP based on the reference TL, an Excel spreadsheet is used to obtain an .atp file data base. Then, a python code is used to access all .atp files and to vary the fault features, obtaining the respective .pl4 file with correct fault parameters, being transformed into COMTRADE records by another python routine. It is important to highlight that ideal VT and CT are considered in this work to minimize the influence of poor frequency response of VTs and saturation problems of CTs (SCHWEITZER *et al.*, 2016). However, these topics are intended to be analyzed in future works.

Still regarding the performed simulations, the SEL-5030 acSELerator Quickset program is used to parameterize the relay settings, which were calculated according to each power system individually, taking into account their particular characteristics according to the relay manual (SEL-T400L INSTRUCTION MANUAL, 2019). Since eight systems are analyzed, as described in Table 5.4, eight different settings are used in the relay. The line propagation velocity is obtained from Table 5.1 and the positive and zero sequence TL impedance are obtained by means of the Line Check routine available in ATP, being described in Table 5.2. Z1MAG and Z1ANG are, respectively, the positive line magnitude and angle impedance, while Z0MAG and Z0ANG are the zero line magnitude and angle impedance, respectively. In addition, to allow the communication between local and remote relays without channel latency, the relays are connect through a short optical fiber link (≈ 2 m).

After the relay configuration via SEL-5030 acSELerator Quickset, another python file is used to generated and send the files in PLAYBACK (.PLY) format to the relay in order to begin the testing procedures. The .PLY file is composed by COMTRADE files in IEEE 2013 pattern format and key variables related to the scheduling and synchronism of the test to be started.

Table 5.2. Impedance Settings

System	Z1MAG (Ω)	Z1ANG (degrees)	Z0MAG (Ω)	Z0ANG (degrees)
1	26.37	82.20	58.50	72.85
2	26.37	82.20	58.51	72.86
3	26.37	82.20	58.20	72.84
4	26.39	82.13	58.38	72.85
5	26.46	81.45	58.71	73.41
6	26.18	81.89	58.92	72.09
7	26.61	81.95	58.79	73.59
8	26.27	80.56	58.77	72.73

Figure 5.1. Relay test methodology.

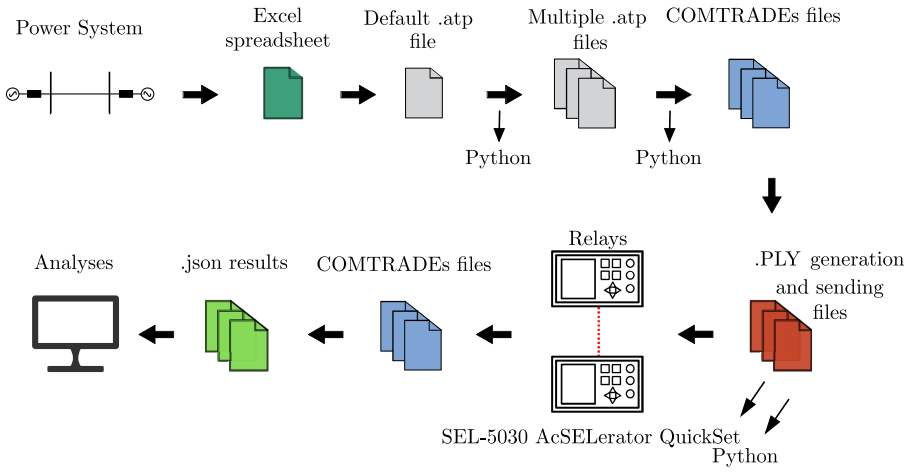

Source: own authorship.

At the end of the performed tests, via python routines, the COMTRADE files are read, estimating the tripping time for each protection function. Then, a JavaScript Object Notation (.json) file is generated in order to assess the operation times and plot the results. Moreover, regarding the fault location methods, the relay outputs for each method are read and the absolute error is calculated for each event.

5.2 EVALUATED POWER SYSTEMS

Two power systems with different configurations have been modeled and simulated in the ATP software. The first analysis is not related to the effects of soil resistivity over the TL, so that a fixed soil resistivity value was initially used. On the other hand, the other set of case studies include the study of the soil resistivity variability along the line length. Thereby, in

order to provide precise data to the second set of studies, the tower configuration, conductors data and soil resistivity values based on a real transmission system located in Brazil were considered.

In order to investigate the impact of frequency-dependence parameters, two different line models are applied. The first line model studied here is the Bergeron model (Be), which considers distributed inductance and capacitance parameters constant in frequency (here set to operate at 60 Hz) and, also concentrate the line losses (DOMMEL, 1969), being in ATP emulated by lumped resistances in 1/4 of its value at both ends and half resistance in the middle of the line (DOMMEL, 1986). The frequency-dependent studied model is the one developed by JMarti (JM), which emulates the line parameters over a pre-defined frequency range (MARTI, 1982). It is considered, for JM model, nine decades and 60 Hz as reference.

For the first evaluated system configuration, the lines are also simulated accounting for different transpositions schemes, namely: ideally transposed (IdT), real transposition (T) and untransposed (UnT). The IdT consists on a mathematical process that the software carries out in order to maintain the balance between mutual couplings along the line. In addition, aiming to simulate the mutual coupling balance between phases in the same way that happens in the field, the T scheme is modeled, which consists in the use of three transposition blocks dividing the TL into four untransposed sections with the lengths equal to $\frac{1}{6}$, $\frac{1}{3}$, $\frac{1}{3}$ and $\frac{1}{6}$ of the total line length. As a result, each untransposed line section stand for the same length throughout the TL in each position, guaranteeing the balance between the mutual couplings. Finally, the UnT scheme, conversely, does not considers the mutual coupling uniformity between phases. It is well known that in real power systems, it is not recommended to build UnT in long TL, but it is analyzed in this work.

All the TL are modeled via ATP Line Constants (LCC) routine. This routine calculates the TL parameters, which are necessary to carry out electromagnetic transient studies, requiring the knowledge of conductors geometric arrangement and their electrical characteristics, as well as the tower geometry and soil resistivity (DOMMEL, 1986; LEUVEN, 1987).

5.2.1 Case Study System

The case study system is modeled with the aim to perform more general studies related to TW propagation patterns, identifying those models that lead simulations to be closer to real world-scenarios. As there is a gap in the literature regarding to TW propagation pattern analysis, this assessment intends to fill this gap and uses this understanding to support future studies related to TW-based functions.

At this study stage, lines modeled as Be and JM are considered, accounting for IdT, T and UnT schemes and with homogeneous soil, i.e., the same soil resistivity value is considered along the TL, resulting in six different systems in total. These systems present TL 210 km long and sources operating at 230 kV/60 Hz, such as depicted in Figure 5.2, illustrating T systems in (a) and IdT and UnT in (b). Also, Figure 5.3 illustrates the tower configuration and conductors data from the modeled system.

Figure 5.2. Test systems.

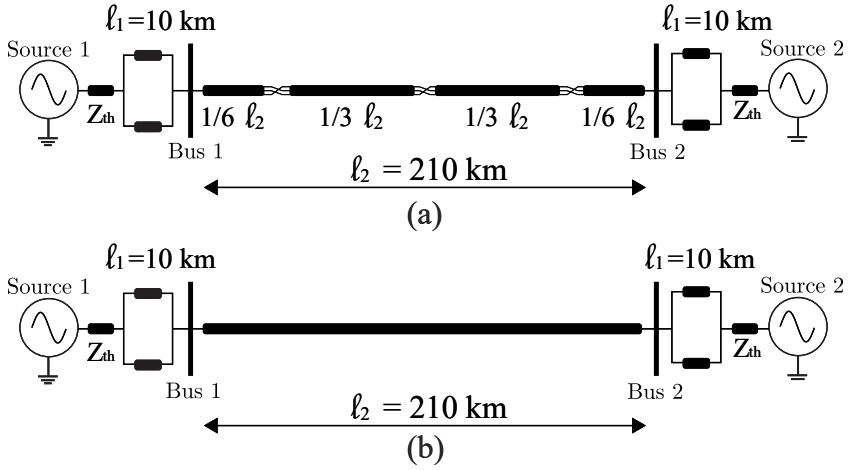

Source: own authorship.

5.2.2 Systems for Studies on Fault Location and Protection Functions

With the aim to analyze the impacts of combinations of TL modeling strategies on fault location and protection functions, here, the system was modeled based on a real transmission system located in northern Brazil, accounting for real tower configuration along with conductors data, as depicted in Figure 5.5, and measured resistivity soil values along the entire line,

Figure 5.3. Tower configuration.

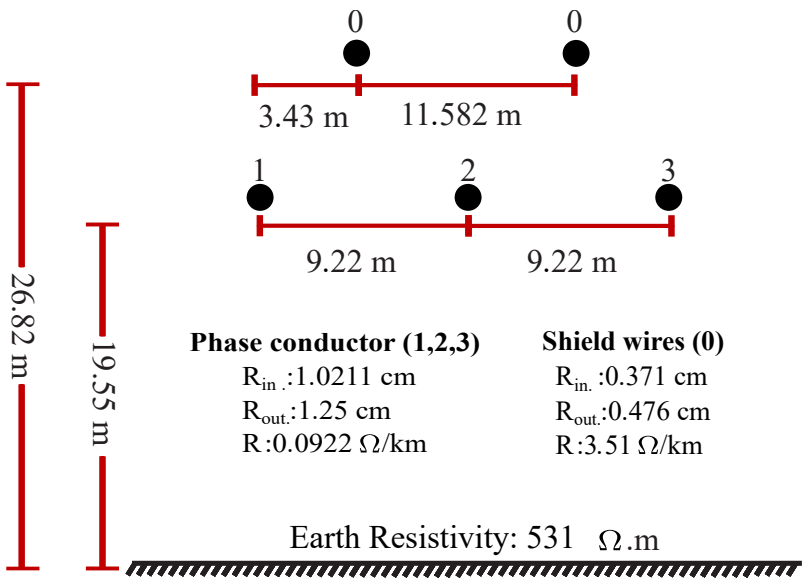

Source: own authorship.

Table 5.3. Soil resistivity values

1º Section (Ω·m)	2º Section (Ω·m)	3º Section (Ω·m)	4º Section (Ω·m)	HS (Ω·m)
92.34	346.95	546.19	79.51	266.25

depicted in Table 5.3. The resistivities values were obtained performing fourteen resistivity measurements, being each measured at depths of 1, 2, 4, 8, 16, 32 and 64 meters and derived from three tests for each measurement. Finally, the average soil resistivity was obtained for each line section.

To evaluate systems with different levels of detail, the combination of Be and JM models, T and IdT schemes and homogeneous (HS) and non-homogeneous soil (NHS) are taken into account. The HS line is modeled with an equivalent soil resistivity obtained by the arithmetic average of the NHS values, while the NHS resistivity values are separated according to the transposition scheme, resulting in four resistivity values for line sections, as shown in Table 5.3. In addition, Table 5.4 describes each evaluated TL according to the modeling characteristic, being System 1 taken as the most simplified model and System 8 as the most realistic one.

The studied TL present the configuration depicted in Figure 5.4, with adjacent lines 70 km long, considering the system operating at 230 kV and 60 Hz and being $l = 235.274$ km.

Table 5.4. Power Systems Schemes

System	Model	Soil	Transposition
1	Be	HS	IdT
2	Be	HS	T
3	Be	NHS	IdT
4	Be	NHS	T
5	JM	HS	IdT
6	JM	HS	T
7	JM	NHS	IdT
8	JM	NHS	T

Figure 5.4. Real system.

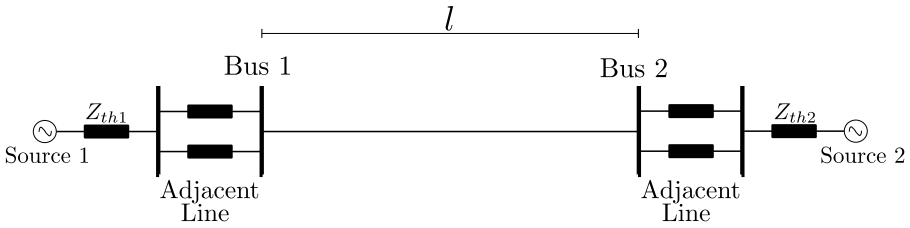

Source: own authorship.

Figure 5.5. Tower configuration.

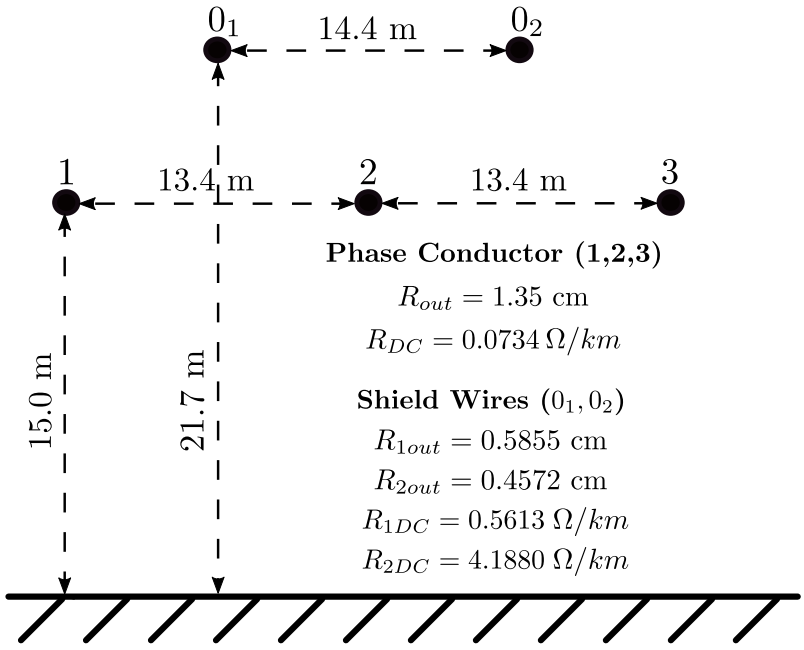

Source: own authorship.

CHAPTER 6

CASE STUDIES AND RESULTS

In this chapter, the performed case studies and the respective obtained results are presented, evaluating the impact of different EMTP line modeling strategies on TW propagation patterns. The effect of different soil resistivity values over TW propagation patterns is also identified along with their impact on propagation velocities in modal domain. Moreover, the influence of EMTP models on the fault location and protection functions described so far are discussed.

6.1 CASE STUDIES

In order to perform the proposed study, initially, a single-phase-to-ground (AG) fault is simulated at a distance of 11.9% of the TL length from the local terminal. Then, the soil resistivity ρ_e is varied for fault distances equal to 10% and 70% of the TL length from the local terminal, being the effect of such resistivity on the TW observed. Finally, the propagation speed is evaluated for TW1, TW2 and TW0 by analyzing the DS filter outputs, comparing the obtained patterns against a real-world record.

6.1.1 Propagation Patterns Comparison

In order to compare the fault-induced transients propagation patterns between the evaluated models, the DS filter outputs are analyzed for the fault at 11.9% of the line length. Firstly, the current-phase signals are considered and, then, the signal is decoupled by means of Clark's transformation. In this study, the modal signals are evaluated, even for UnT lines. Indeed, in real applications, the modal transformation has been applied even when the transmission line transposition is not ideal.

The first incident phase TW wavefront measured in the terminal is illustrated in Figure 6.1

and the respective amplitude and peak instant are listed in Table 6.1. Analyzing the results, it is concluded that the signal from JM arrives at the monitored terminal firstly than in the Be model, i.e., lines modeled according to JM have higher propagation speed than the ones modeled as Be at 60 Hz. In addition, it is noticed that JM signals arrive with larger amplitude than Be signals, attesting that exist differences in the attenuation emulated by each model. It is also concluded that the line model and transposition approaches results in different TW patterns. Even so, deviations related to transposition schemes are not considered critical. On the other hand, considering the line parameters frequency dependence effects, they result in uncertainties on the TW propagation arrival times and amplitudes, which may become an issue to parameter-dependent solutions.

Although, observing the same signal (now accounting only for IdT scheme for the sake of comparison), but considering the zoomed time area in Figure 6.2, it is concluded that, although JM presents larger amplitude for the case depicted in Figure 6.1, it also presents greater attenuation and dispersion over the propagation time than Be line model.

Still analyzing Figure 6.1, it is observed that in Be model there is a second set of phase TW while for JM this second set does not exist. Aiming to investigate such a second set of TW, the signal is decoupled and the respective TW1 and TW0 are shown in Figure 6.3. According to Figure 6.3, it is noticed that this second set of Be TW corresponds to the respective TW0 from

Figure 6.1. First incident phase TW at local terminal.

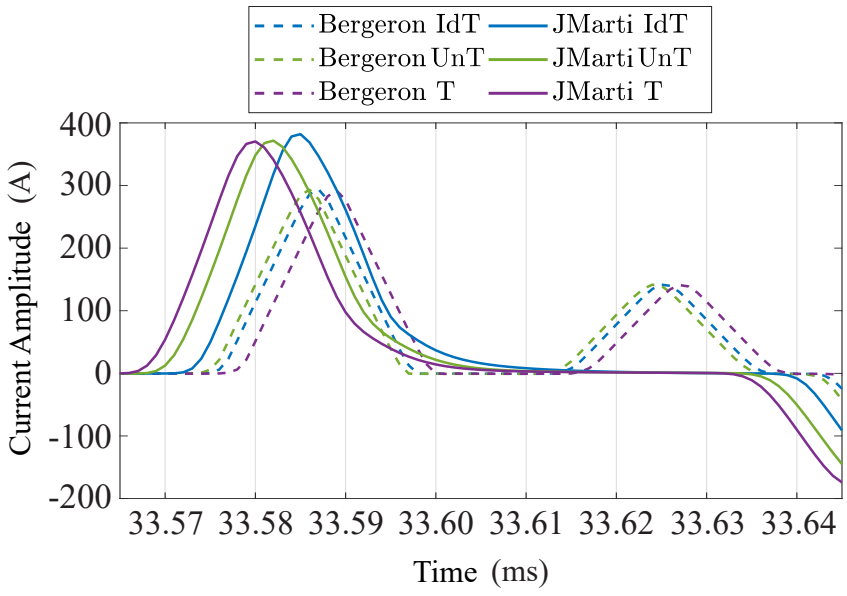

Source: own authorship.

Table 6.1. Amplitude and TW peak instant.

TL modeling scheme	Time (ms)	Amplitude (A)
JMarti T	33.580	370.373
JMarti UnT	33.582	371.659
JMarti IdT	33.585	382.079
Bergeron UnT	33.586	293.405
Bergeron IdT	33.587	293.780
Bergeron T	33.589	291.850

Figure 6.2. Phase TW for a larger time window.

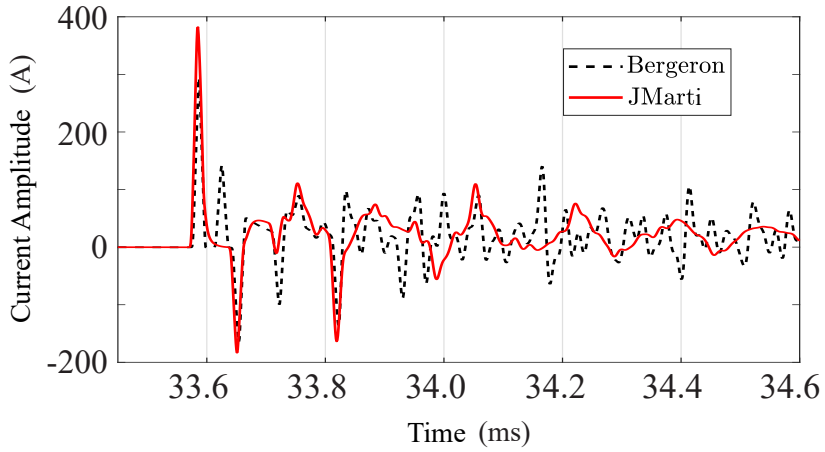

Source: own authorship.

the phase signals, being concluded that TW propagate much slower in Be (60 Hz) model than in JM model. As a consequence, this significant difference in the TW0 propagation velocity for Be line model results in relevant differences in phase transients and, especially, in ground mode transients. Therefore, the use of phase TW when the TL is modeled as Be produces false peaks that can result in relevant simulation differences (CHALANGAR *et al.*, 2020) with respect to the JM model when wavefronts that take place after the first incident TW are required to be analyzed.

In order to verify which line model originates TW patterns closer to those found in the field, Figure 6.3 is compared with Figure 6.4. Figure 6.4 presents a real-world TW1 and TW0 record reported by Lopes *et al.* (2019b), which refers also to a single-phase-to-ground fault with similar features. It is concluded by visual inspection that JM model reproduces more accurately real-world fault-induced transients, as expected.

Figure 6.3. Modal TW.

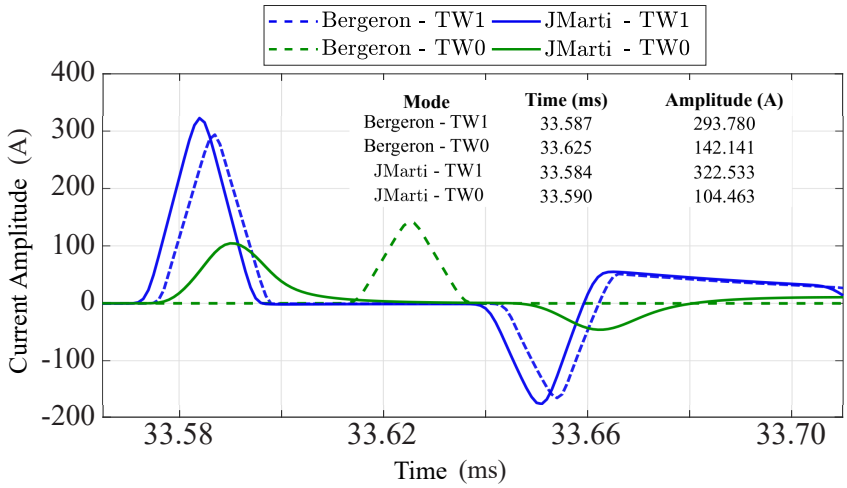

Source: own authorship.

Figure 6.4. Real-world TW1 and TW0 record reported by Lopes *et al.* (2019b).

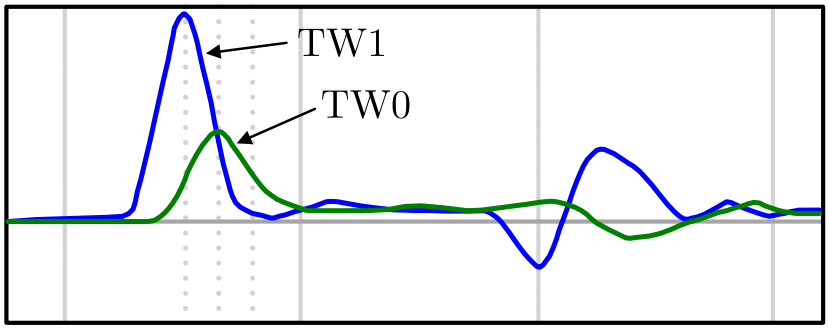

Source: own authorship.

6.1.2 Soil Resistivity Evaluation

The effect of soil resistivity variation on TW propagation patterns is analyzed in this section. Four different soil resistivity values are evaluated, namely: 300, 531, 2100 and 4100 $\Omega \cdot m$. These values cover a wide range of soil types, allowing a reliable analysis. In this study, only the IdT scheme is taken into account for Be and JM models, but for the sake of comparison, Be and JM signals are depicted in different figures. Figure 6.5 shows the TW1 and TW0 for a fault at 10% of the line length from the monitored terminal considering the JM model, while Figure 6.6 shows the same scenario, but taking into consideration the Be model.

Analyzing Figures 6.5 and 6.6, it is noticed that the soil resistivity variation effects are more relevant for TW0 than for TW1. It is also observed that such effects impact more on wavefronts

Figure 6.5. Effect of soil resistivity on modal TW for JM modal a fault at 10% of the line length.

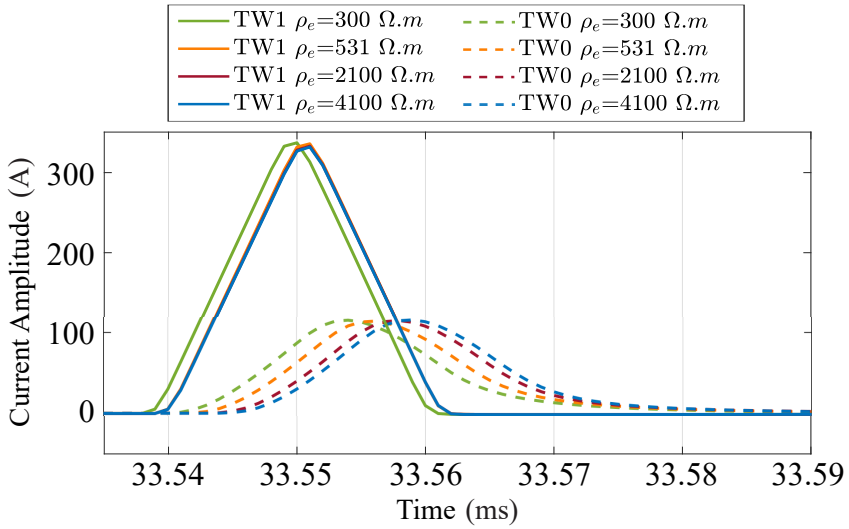

Source: own authorship.

Figure 6.6. Effect of soil resistivity on modal TW for Be modal a fault at 10% of the line length.

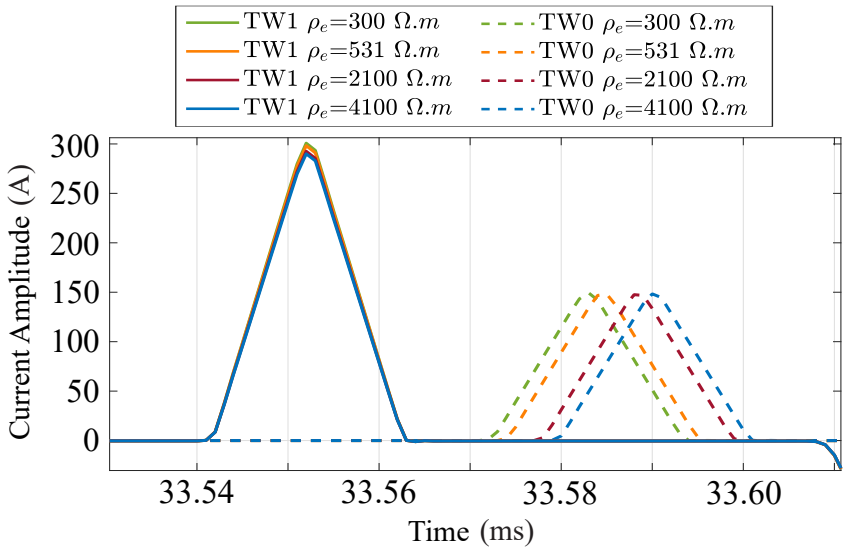

Source: own authorship.

arrival times that on magnitudes, representing a source of uncertainties for TW propagation velocities. Finally, it is concluded that the greater the soil resistivity value is, the grater is the delay imposed on TW0.

Aiming to validate the impact of soil resistivity on modal TW, a fault is simulated now at 70% of the line length from the monitored terminal. The record obtained for JM model is depicted in Figure 6.7, whereas the results obtained for the Be model are shown in Figure 6.8. From these figures, the previous results are validated, confirming that the attenuation and dispersion verified in JM model simulations are much greater than those observed in Be model.

Figure 6.7. Effect of soil resistivity on modal TW for JM modal a fault at 70% of the line length.

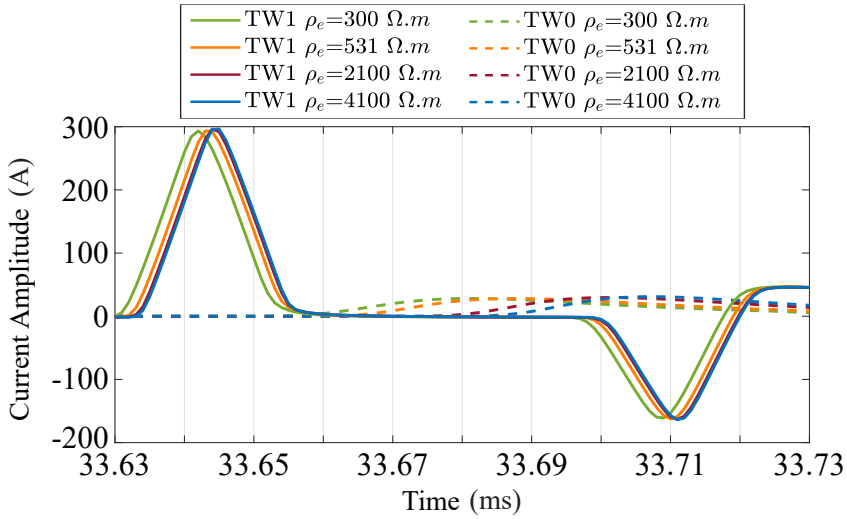

Source: own authorship.

Figure 6.8. Effect of soil resistivity on modal TW for Be modal a fault at 70% of the line length.

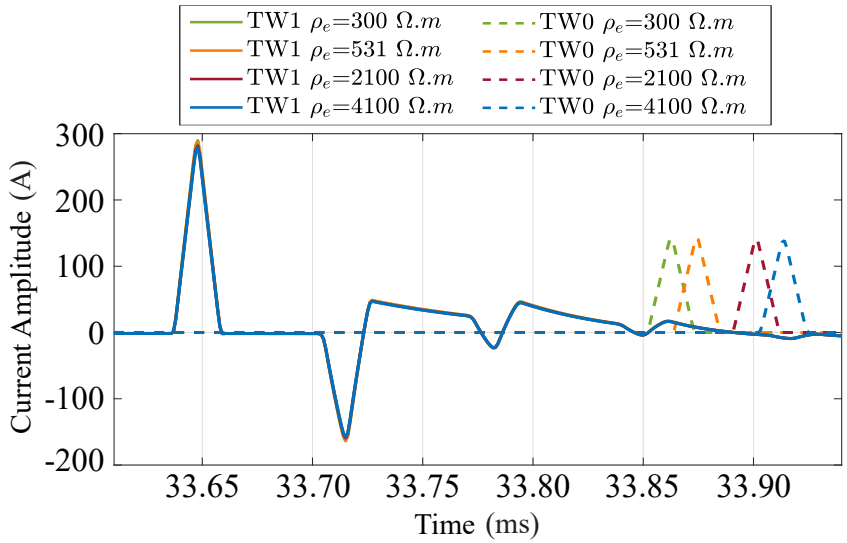

Source: own authorship.

6.1.3 Propagation Speed Analysis

To better understand the results obtained so far, the modal TW propagation speeds are evaluated over the frequency spectrum, considering a frequency range from few dozens of hertz until the order of megahertz. To do so, Figure 6.9 represents this analysis for TW0, TW1 and TW2. It is concluded that aerial modes have a very similar pattern, without relevant variations

Figure 6.9. Modal TW velocity analysis in frequency.

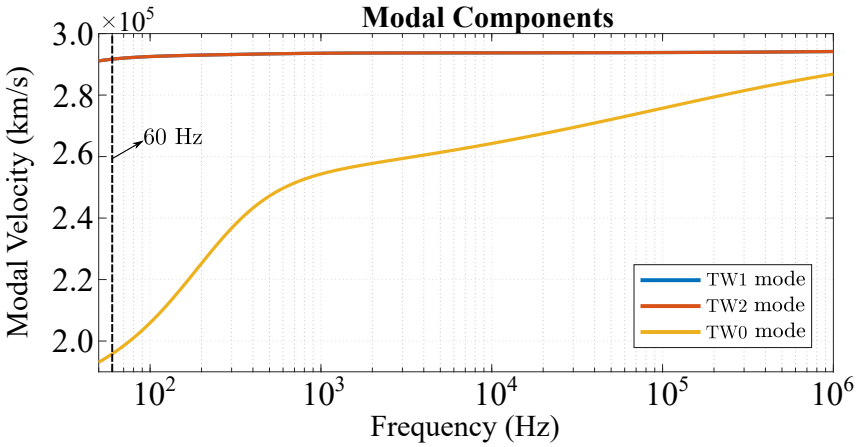

Source: own authorship.

Figure 6.10. TW1 velocity analysis in frequency.

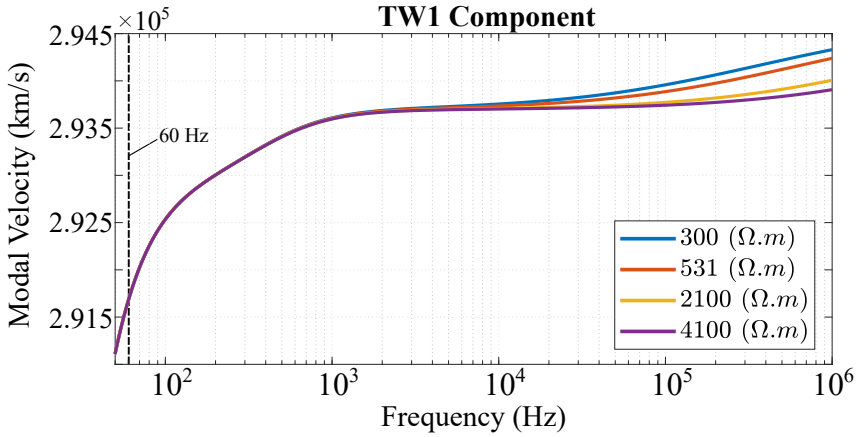

Source: own authorship.

in their propagation velocities, being TW1 and TW2 superimposed on the considered figure scale. In addition, at the fundamental frequency (60 Hz), the TW0 velocity is much lower than the aerial TW, which explains the reason that led the Be model to deviate more from the TW0 results by using JM model. On the other hand, aerial mode TW do not vary significantly their velocities over the frequency, while the propagation speed for ground TW increases as the frequency increases. Thereby, the use of frequency independent line parameters may result in significant errors if ground mode transients are expected to be analyzed. Moreover, when the mixing mode takes place, errors in TW0 may yield discrepancies in TW1 reflections in relation to what is expected to occur in real systems.

To further investigate theses results, Figures 6.10 and 6.11 show the TW1 and TW0 modal velocities, respectively, over the frequency spectrum, but now varying the soil resistivity.

Figure 6.11. TW0 velocity analysis in frequency.

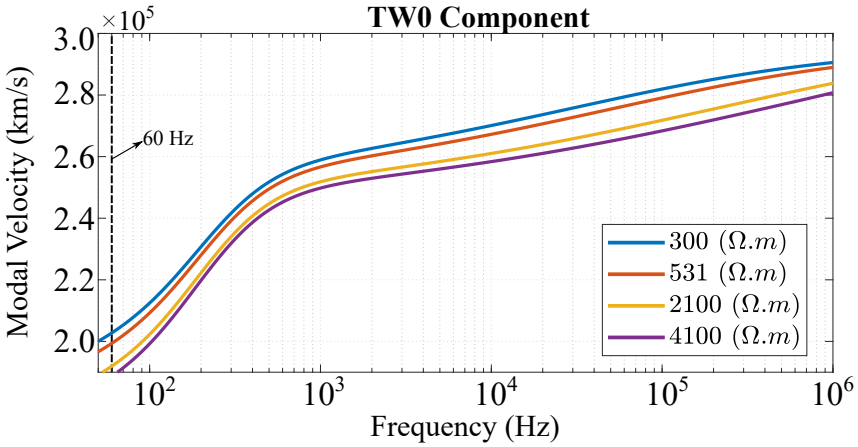

Source: own authorship.

From Figures 6.3 and 6.11, it is concluded that the resistivity impacts all modal components. Nevertheless, TW0 is affected over all the frequency spectrum, while TW1 velocity is more affected at higher frequencies.

6.2 IMPACTS ON FAULT LOCATION AND PROTECTION FUNCTIONS

In order to further investigate the influence of TL modeling strategies on fault location and protection functions performance, single-phase-to-ground faults (AG) and double-phase faults (BC) are simulated in ATP. Here the TL modeling aspects for the Systems depicted in Table 5.4 are considered, being System 1 always used as the reference for the sake of comparison, allowing the identification of modeling complexity aspects that affect the analyzed methods. Firstly, the computational simulations are carried out, followed by the relay testing procedures.

6.2.1 Computational Simulations

The proposed study considers the fault distance varying from 3% up to 96% of the line length with steps of 3%, i.e., 32 fault distances are considered for each system and fault type. Hence, considering these distances along with the eight power systems and two simulated fault types, a total of 512 simulations are performed. For this analysis, C1T, C2T, GIL and FLO methods are taken into account.

Aiming to properly identify the effects of each modeling approach on TWFL methods, the assessment is divided in three parts. Firstly, the systems are compared varying only one modeling variable per time, and then, all modeling characteristics are combined, being these results presented as scatter plots. Finally, in order to obtain a better quantitative overview on the results, all absolute errors obtained from the analyzed TWFL methods are shown in a boxplot format.

In the literature, in the knowledge area related to fault location on transmission lines, scatter plots have been used as a way to contrast the performance of methods under different scenarios, such as depicted in (LOPES *et al.*, 2018; LOPES *et al.*, 2019b; SCHWEITZER *et al.*, 2016). To better understand the scatter plot, it is important to notice that it presents a coincidence diagonal line, which represents the region on which both evaluated scenarios present similar performance. Furthermore, the scatter plot presents two areas, above and below the diagonal line. In this work, points on the superior region (pink area) represent cases in which the modeling simplifications in System 1 increase the TWFL errors, whereas points on the inferior region (yellow area) represent scenarios in which the modeling simplifications in System 1 decrease the TWFL errors. One should notice that the Y-axis is taken as the reference for the sake of comparison, being always associated to the most simplified system model (System 1) among those evaluated in this thesis.

6.2.1.1 Individual analysis of modeling variables

In this section, the influence of transposition schemes is analyzed, comparing Systems 1 and 2; the soil heterogeneity is assessed, comparing Systems 1 and 3; and finally, Systems 1 and 5 are compared to evaluate the impact of TL parameters frequency dependence. To improve figures legibility, errors greater than 1 km were classified as outliers, not being shown in the figures.

Analyzing Figure 6.12, it can be concluded that the application of real transposition schemes increase errors when contrasted with IdT schemes. This can be explained by the fact that, for lines modeled as IdT, the propagation velocity is always the same along the entire line. Nevertheless, when a T line is considered, the propagation speed may present differences for

Figure 6.12. Analysis 1 - absolute error between System 1 and System 2, analyzing transposition schemes.

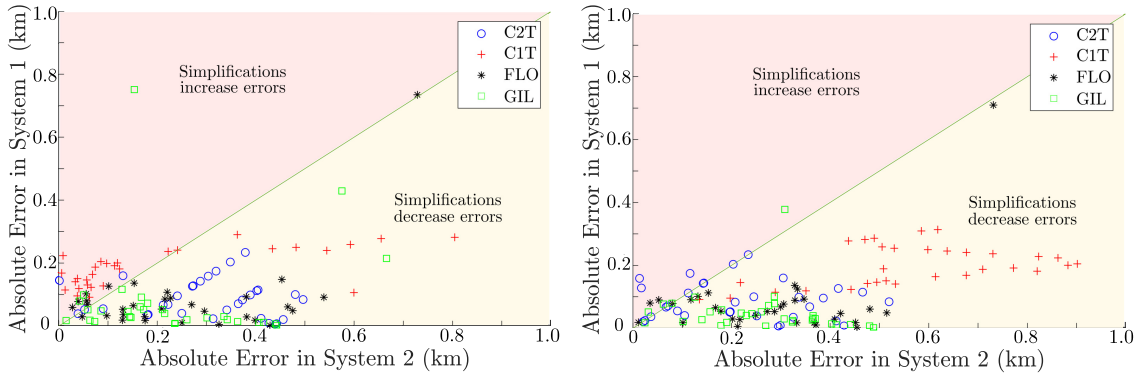

(a) AG Fault (b) BC Fault

Source: own authorship.

Figure 6.13. Analysis 2 - absolute error between System 1 and System 3, analyzing soil heterogeneity.

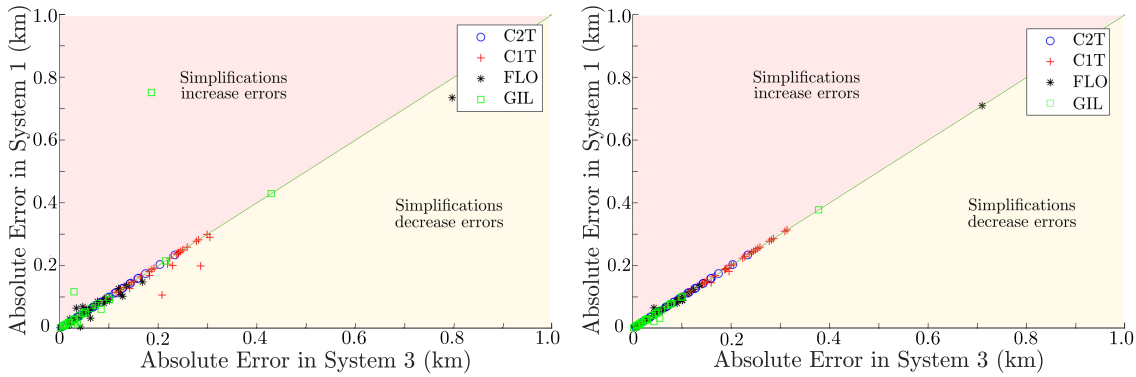

(a) AG Fault (b) BC Fault

Source: own authorship.

each untransposed line section, so different v values can be verified in each phase, resulting in uncertainties that can affect the TWFL methods performance.

From Figures 6.13(a) and 6.13(b), it is concluded that modeling the soil as NHS or as HS does not significantly affect the TWFL methods applied in this study, since most points are located on the diagonal coincidence line. The previous studies helps to understand this, once it was shown that the soil resistivity has great impact over the TW0, but not on aerial mode wavefronts TWs, which are only slightly affected. In addition, all the studied methods are based on TWs, so that the soil heterogeneities do not notably affect the TWFL methods errors.

Figure 6.14 shows that most points are on the yellow area, i.e. for a power system modeled as Be, errors are smaller than those observed for a system with frequency-dependent parameters. In addition, it is seen that, in general, GIL and FLO methods present better performance

Figure 6.14. Analysis 3 - absolute error between System 1 and System 5, analyzing TL model schemes.

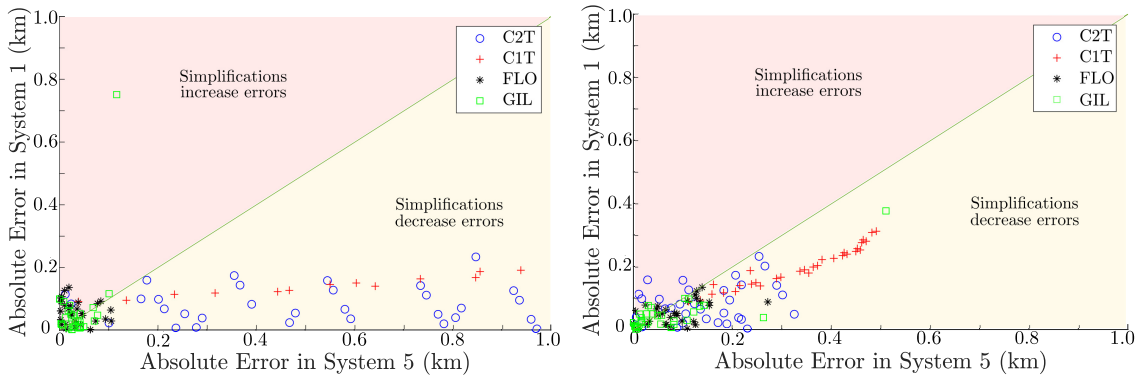

(a) AG Fault (b) BC Fault

Source: own authorship.

than C1T and C2T. This performance is explained by the fact that FLO and GIL do not require TW propagation velocity settings, overcoming uncertainties caused by line parameters deviations. Moreover, a noteworthy finding is that TWFL errors related to grounded fault cases are larger and more dispersed than ungrounded fault cases, since the mixing mode only occurs for faults involving the ground, leading different modes to be coupled in phase-to-ground fault cases when reflections and refractions occur at the fault point (PHADKE; THORP, 2009). Hence, the mixing mode phenomenon results in additional distortions on the analyzed signals, mainly affecting TWFL methods that require the detection of TW reflected or transmitted from/through the fault (DEMAGALHAESJUNIOR; LOPES, 2021).

6.2.1.2 Combined analysis of modeling variables

Continuing the studies, the TL modeling characteristics are combined in the analyzed scenarios. Basically, two features are combined per time, maintaining the remaining ones fixed. Finally, all three features analyzed in this work are contrasted. Initially, the transposition scheme along with soil heterogeneities are combined and analyzed in Figure 6.15. The methods performance is quite similar to the presented in Figure 6.12, in which only the transposition scheme is studied. Hence, since the NHS demonstrated to have no relevant impact over the TWFL errors, it is concluded that the T scheme is the most critical feature in this scenario.

It is observed in Figure 6.16 that, when frequency-dependent line model is combined with real transposition scheme, the TWFL errors dispersion increase. This performance is indeed

Figure 6.15. Analysis 4 - absolute error between System 1 and System 4, analyzing soil and transposition schemes.

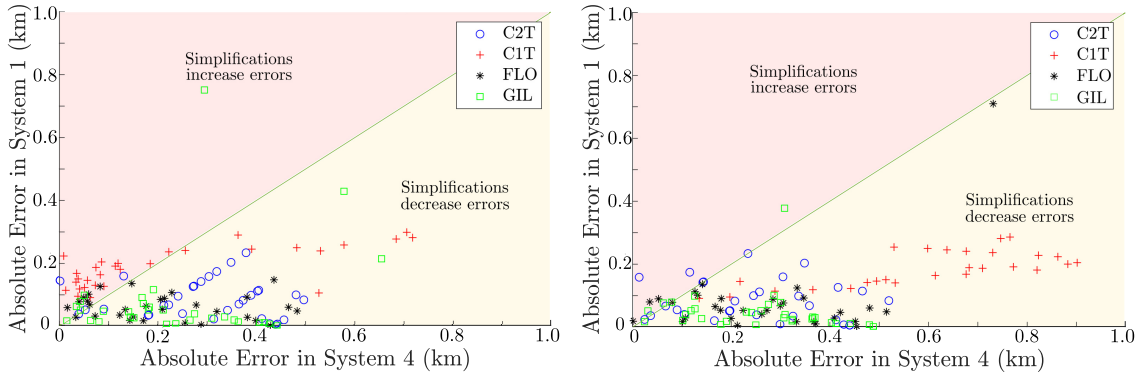

(a) AG Fault (b) BC Fault

Source: own authorship.

Figure 6.16. Analysis 5 - absolute error between System 1 and System 6, analyzing TL model and transposition schemes.

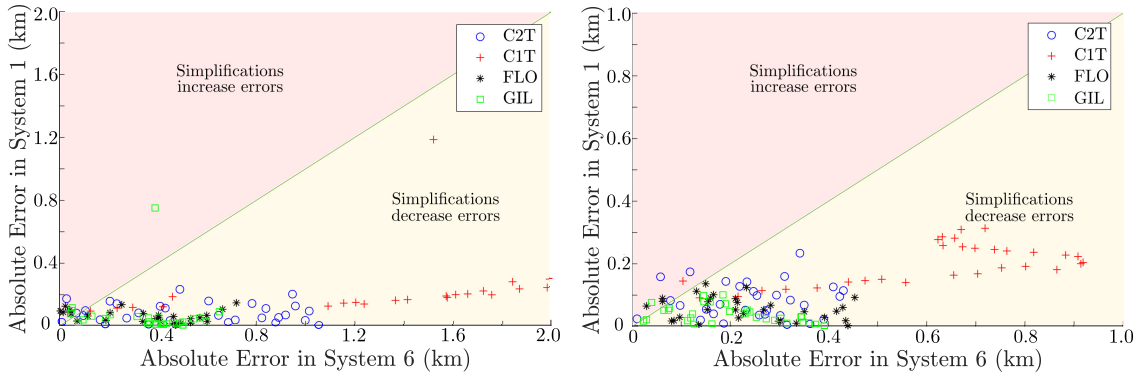

(a) AG Fault (b) BC Fault

Source: own authorship.

expected, since this analysis correspond to the same scenario analyzed in Figures 6.12 and 6.14. Thus, it is concluded that the use of more realistic models increase fault location errors. Furthermore, analyzing Figures 6.16(a) and 6.16(b), it is also observed that the errors are greater for AG faults than for BC short-circuits, being concluded that the use of JM model affects more the TWFL accuracy for grounded faults.

The mixing mode phenomenon can be also noticed in Figure 6.17, in which the line model is combined with soil features. Indeed, a higher dispersion level takes place in the TWFL errors in Figure 6.17(a) if compared with Figure 6.17(b). Besides, it is observed that in Figure 6.17, the errors are more dispersed than in Figure 6.14, demonstrating that soil heterogeneity also have a slightly impact over TWFL errors when JM model is applied, whereas for Be line model

it does not present significant influence.

Finally, line model, soil heterogeneity and transposition scheme are combined and evaluated, being the obtained errors shown in Figure 6.18. In this analysis, the most simplified system model is compared to the one considered as the most realist model. It is seen that most points take place in the yellow area, attesting that a more complex TL modeling approach indeed pose more difficulties on TWFL methods. Even so, from the presented cases, it can be concluded that some scenarios present a different behavior, unlike the preliminary expectations, showing that simplifications can also negatively affect the testing procedures in specific scenarios.

Figure 6.17. Analysis 6 - absolute error between System 1 and System 7, analyzing TL model and soil schemes.

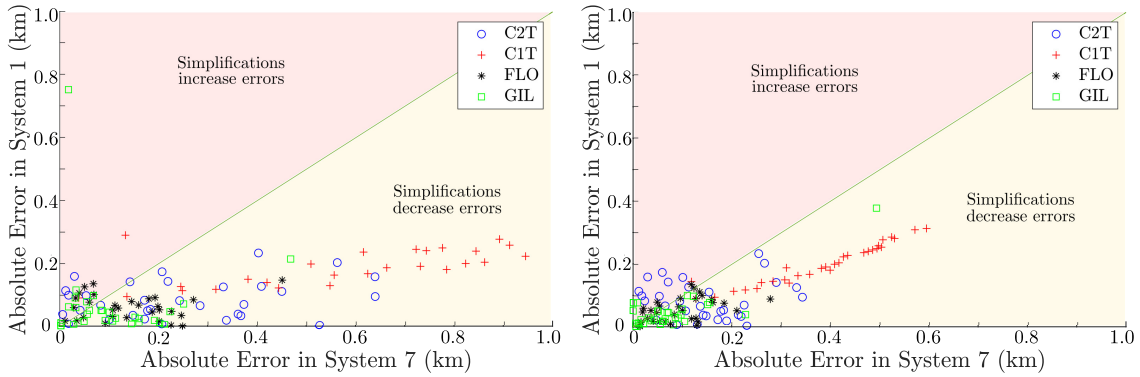

(a) AG Fault (b) BC Fault

Source: own authorship.

Figure 6.18. Analysis 7 - absolute error between System 1 and System 8, analyzing TL model, soil and transposition schemes.

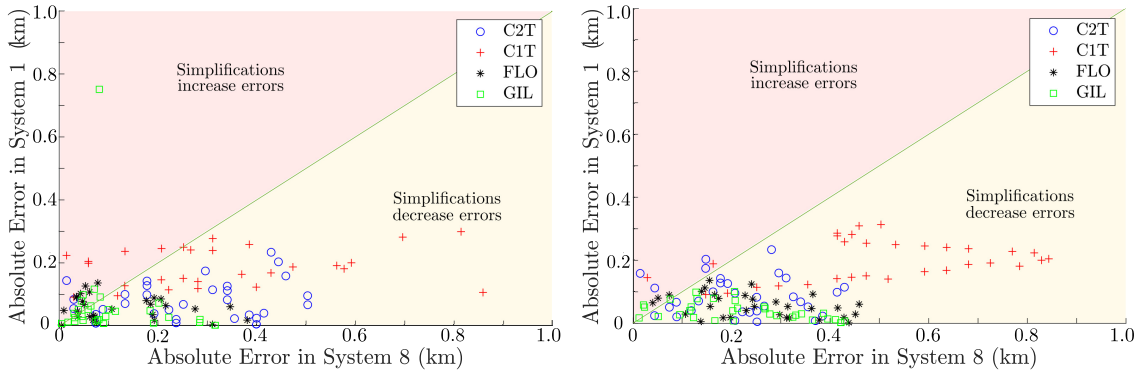

(a) AG Fault (b) BC Fault

Source: own authorship.

6.2.1.3 Absolute errors comparison

To provide an overview on the obtained results, boxplots are generated from the TWFL absolute errors for each method. It is important to notice that few outliers found with errors greater than 3 km for AG fault cases in Figure 6.19 and 2 km for BC fault cases in Figure 6.20 are not shown, without loss of reliability of the obtained conclusions.

From Figure 6.19, it is seen that the error median is below 2 km for all cases. In addition, an important conclusion is that C1T method presents greater errors due to the challenging procedure of identifying the fault-reflected TW. It is also observed that JM model presents greater impact on errors in C1T and C2T methods due the need of line parameters settings. Besides, is is also noticed that the systems with even code numbers (the ones modeled with real transposition scheme) present larger TWFL errors than those with odd code numbers, which attests the effects of transposition schemes, specially on FLO and GIL techniques.

Observing Figure 6.20 it is noted that the median values are below 1 km for all systems and for all TWFL techniques. On the other hand, the errors in Figure 6.19 are larger, proving that the mixing mode effect is indeed critical in grounded fault cases. Furthermore, the impact of transposition schemes is also verified in all techniques in the Figure 6.20.

Aiming to facilitate the quantitative TWFL error analysis, average errors are presented in

Figure 6.19. Boxplot representing the absolute errors for all power systems schemes separated by TWFL methods considering AG fault.

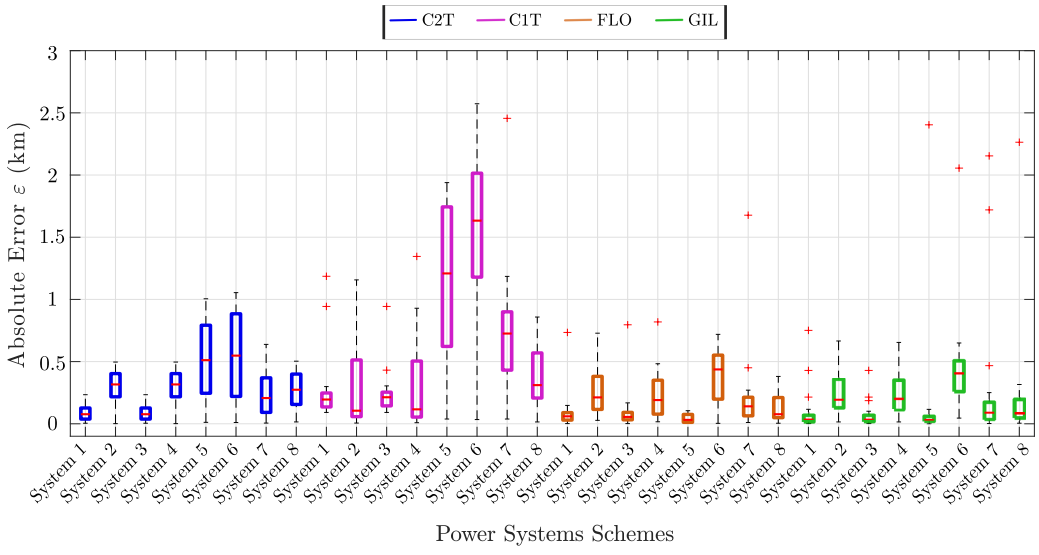

Source: own authorship.

Table 6.2 for each power system studied and in Table 6.3 for each evaluated TWFL technique, considering the cases in which the methods operated as expected. Analyzing both tables, double-phase faults indeed tend to present lower average errors than single-phase-to-ground faults. It can also be concluded that systems modeled with more realistic characteristics tend to result in larger TWFL errors. However, such behavior is not a rule. Since the average errors for C1T method are noticeably higher than for the others methods, as observed in Table 6.3, it is confirmed that TW reflected detection is a source of TWFL errors. Also, it is demonstrated that methods that do not require TL electrical parameters commonly result in more accurate fault location estimations.

Figure 6.20. Boxplot representing the absolute errors for all power systems schemes separated by TWFL methods considering BC fault.

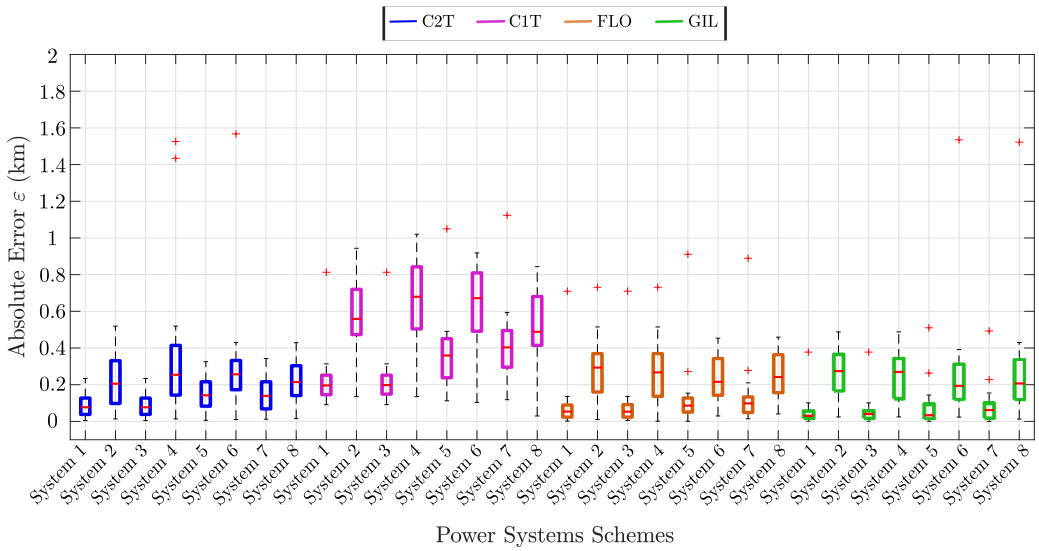

Source: own authorship.

Table 6.2. Average errors per system

System	Average error for AG fault (km)	Average error for BC fault (km)
1	0.1149	0.1076
2	0.4642	0.3337
3	0.1078	0.1084
4	0.2426	0.4681
5	0.7377	0.1715
6	0.7074	0.4145
7	0.3843	0.1875
8	0.5545	0.3571

Table 6.3. Average errors per TWFL technique

TWFL method	Average error for AG fault (km)	Average error for BC fault (km)
C1T	0.8127	0.5208
C2T	0.2962	0.1976
FLO	0.2781	0.1983
GIL	0.2698	0.1576

6.2.2 Protective Relay Testing Cases

In this part of the proposed studies, solid faults are simulated for all eight systems described in Table 5.4. The evaluation is performed with the fault distance varying from 1% up to 99% of the line length with steps of 1%, i.e. considering eight systems, two fault types and 99 fault distances per system, accounting for each fault type, a total of 1,584 scenarios are simulated. The obtained results are presented in two stages. Initially, four fault location methods embedded in the relay are analyzed and the obtained absolute errors are compared for all events by the application of a boxplot for each fault type separately. It is important to notice that, in this part, the same acronyms used in the relay are taken into account, namely: SETWFL, DETWFL, SEZFL and DEZFL, being SETWFL and DETWFL similar to the C1T and C2T methods, respectively. Then, the relay tripping times are obtained, allowing a comparative analysis, for all evaluated system and all protection functions available in the assessed time-domain relay. These results are presented by means of probability density graphics for each function.

6.2.2.1 Fault location studies

When fault location is carried out by the relay, it can return either an estimated fault location value or the character string '$$$$$$$' to represent cases in which the TWFL method was unable to identify fault location. For the sake of the proposed studies, the events in which the relay was not able to estimate fault location were not taken into account. In addition, only errors smaller than 5% of the line length were considered as valid, being the remaining ones not taken into account in this work. Indeed, Z-based methods tend to yield larger errors values than TW-based ones, and the typical accuracy of Z-based methods is of about 5% of the

line length (ZIMATH *et al.*, 2010). Furthermore, the real number of events considered for error evaluation of each power system are also depicted along with boxplots in bars format. By doing so, one can verify the number of valid cases (which would be useful in practical procedures) and their respective error levels.

The difference in the number of valid events for the SETWFL technique among the other methods, as observed in Figure 6.21, is relevant, which is a consequence of the challenging task of detecting TW reflected from the fault point. Still analyzing the SETWFL method, it is observed that the amount of converging valid cases for the systems modeled as Be are more significant when compared to JM, in which just few cases are taken into account. This difference is explained by the dispersion and attenuation during the TW propagation generated by the frequency-dependence of line parameters, as previously demonstrated in this work. It implies in additional difficulties to properly identify the reflected waves, resulting in greater errors. At the same time, though, DETWFL, which requires only the first incident TW detection, and SEZFL and DEZFL, which are Z-based methods, they resulted in a great number of valid cases in almost all simulated scenarios. In addition, in this analysis, the larger impact of real transposition schemes over the TWFL errors is also evidenced, since higher errors for even systems are observed (the ones modeled as T transposition). Furthermore, as expected, the

Figure 6.21. Boxplot representing the absolute errors separated by fault location methods and bars presenting the number os scenarios taken into account for all power systems schemes considering AG fault.

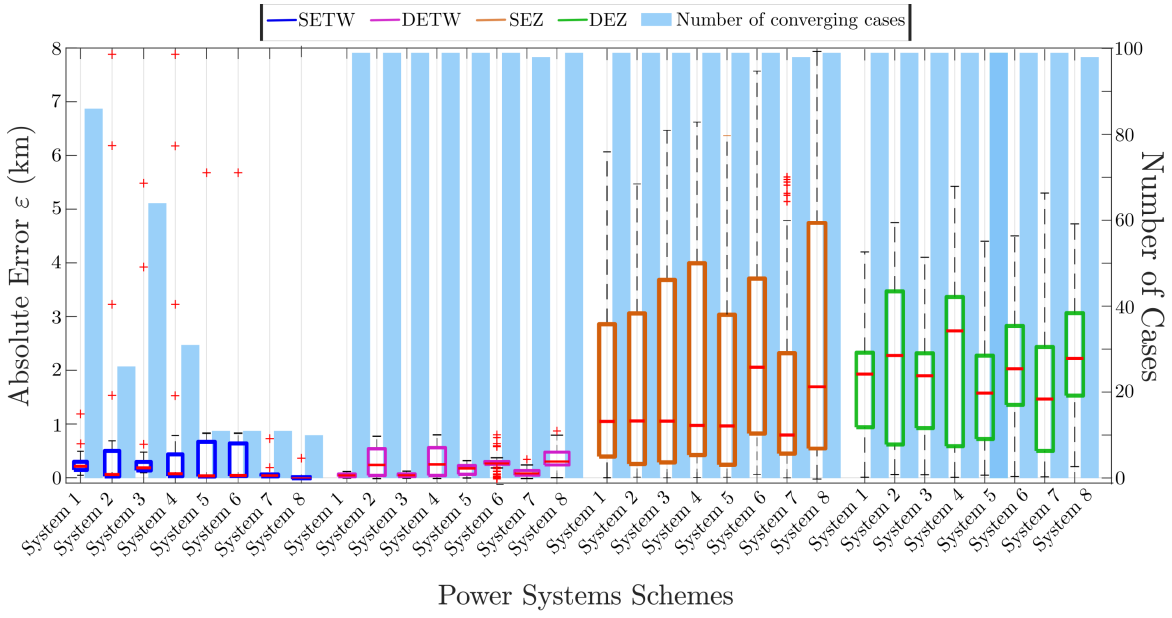

Source: own authorship.

Figure 6.22. Boxplot representing the absolute errors separated by fault location methods and bars presenting the number os scenarios taken into account for all power systems schemes considering BC fault.

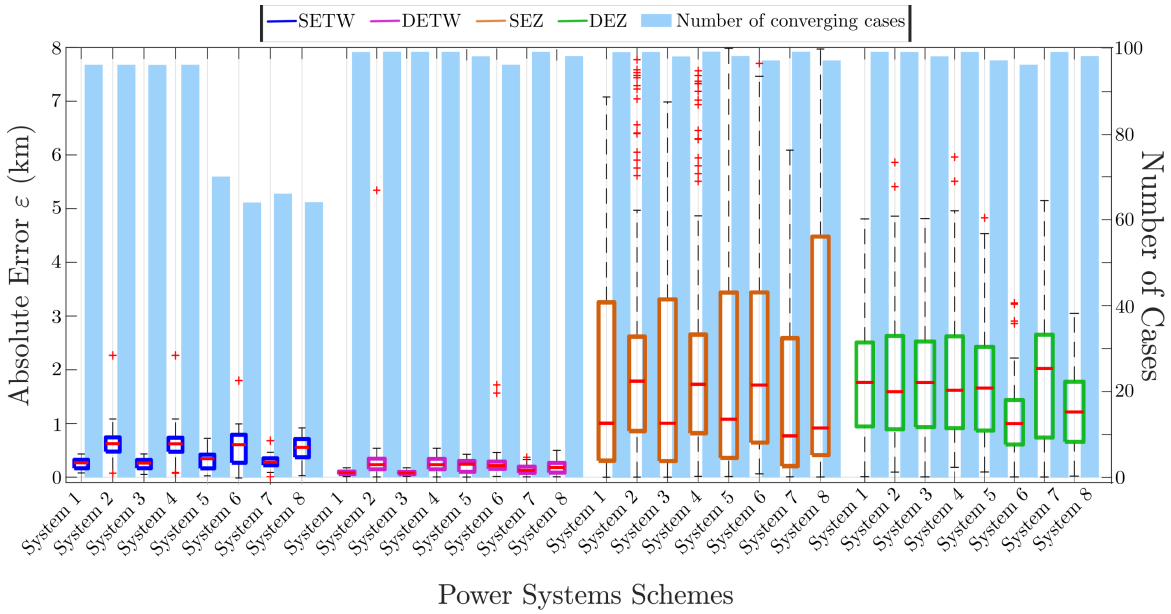

Source: own authorship.

Z-based methods present greater errors than TW-based techniques.

Analyzing Figure 6.22 and comparing with Figure 6.21, it is seen that the number of converging cases within the 5% accuracy increase in a noticeable way for SETWFL due to the fact that the mixing mode phenomenon does not occurs for double-phase faults, so that the method can present a better performance. The conclusions obtained for T scheme effect over the errors is also observed here. Nevertheless, no relevant impact could be observed for the Z-based methods.

6.2.2.2 Protection functions studies

It is noteworthy to point out that the evaluations performed here are done considering only the local terminal and the results are shown as the operation time in function of the fault location. In addition, the probability density distribution function for the operation time of the evaluated time-domain protection element is presented, considering both fault types and all eight systems. It is also important to highlight that only events in which the protection functions were sensitized were taken into account for the studies.

The relay tripping time for each protection element regarding the simulated fault events is

Figure 6.23. TD21 Operation time as a functions of the fault distance.

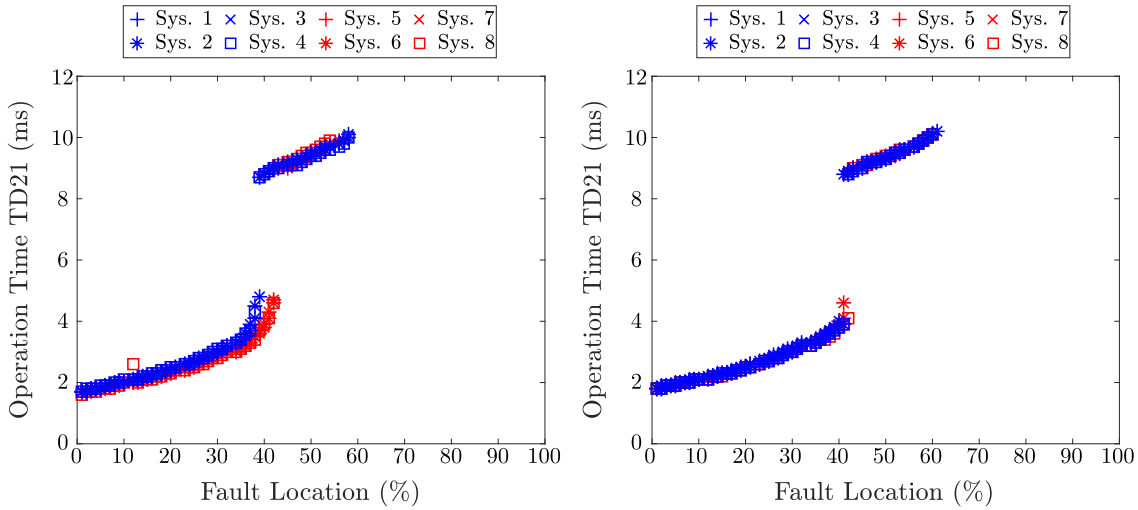

(a) AG Fault (b) BC Fault

Source: own authorship.

Figure 6.24. TD32 Operation time as a functions of the fault distance.

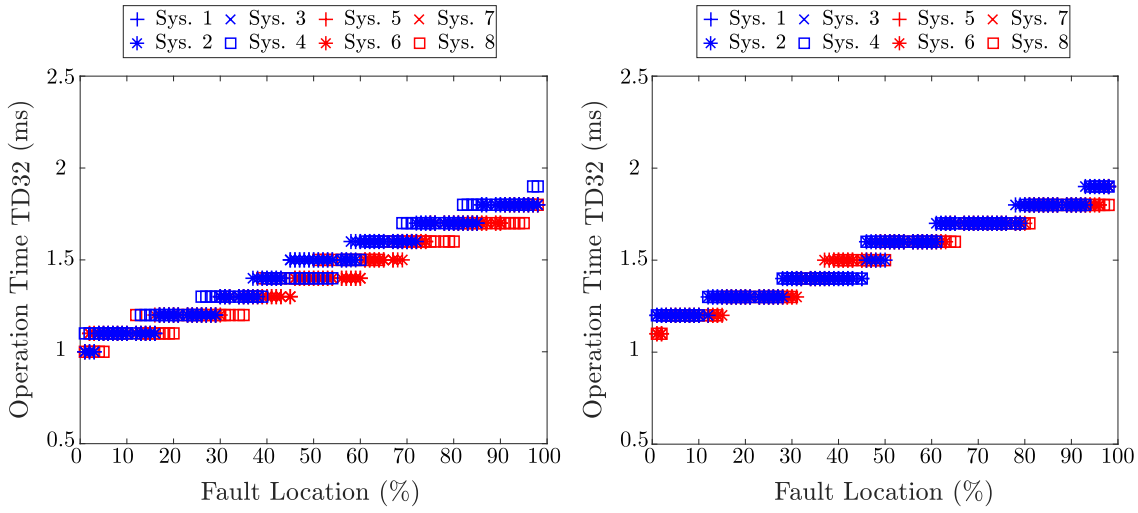

(a) AG Fault (b) BC Fault

Source: own authorship.

depicted in Figures 6.23, 6.24, 6.25 and 6.26, being the blue color applied for Be systems and red color for the JM systems, for the sake of visibility. From all figures, it is noticed that for each element, the operation time patterns are maintained for AG and BC fault cases. In relation to the modeling line approaches, few differences are noticed, but most points are overlapped. Besides, the obtained performance of all functions were as expected, being in accordance to SEL-T400L Instruction Manual (2019), Lopes *et al.* (2020).

Figure 6.23 shows that the fault detection happens until 60% of the line length approxi-

mately, however, the element ensures high-speed tripping protection only until 40% of the line length. Instead, TD32, as depicted in Figure 6.24, ensures the fault detection along the entire TL, resulting on fast operation times between 1 and 2 ms, which increases as the fault gets far from the monitored terminal.

TW-based protection elements ensure faster operation times than TD functions. The operation time pattern for TW32 is similar to the pattern obtained for TD32, however, the tripping time do not exceed 0.8 ms, as observed in Figure 6.25. Although, Figure 6.26 shows that

Figure 6.25. TW32 Operation time as a functions of the fault distance.

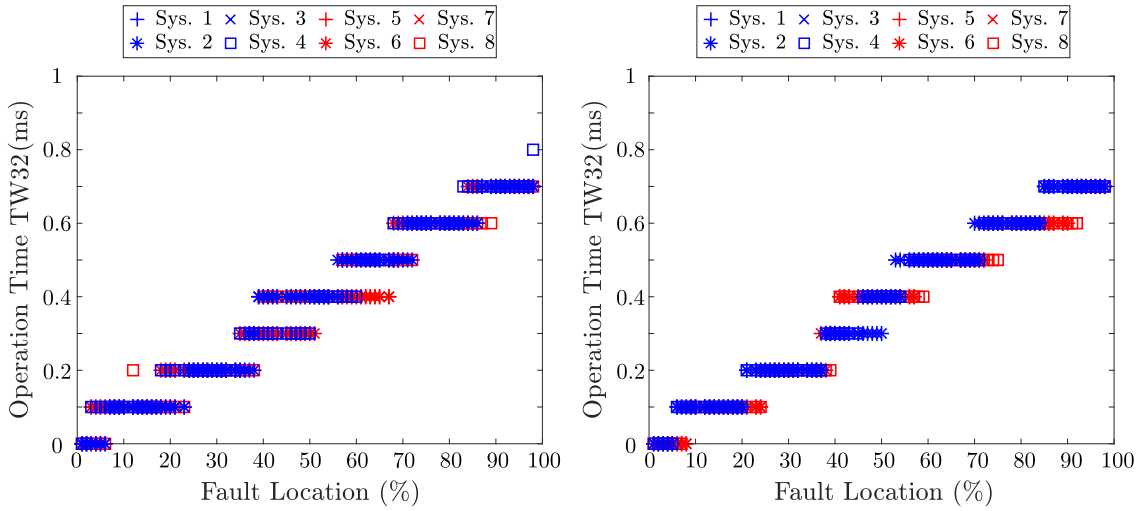

(a) AG Fault (b) BC Fault

Source: own authorship.

Figure 6.26. TW87 Operation time as a functions of the fault distance.

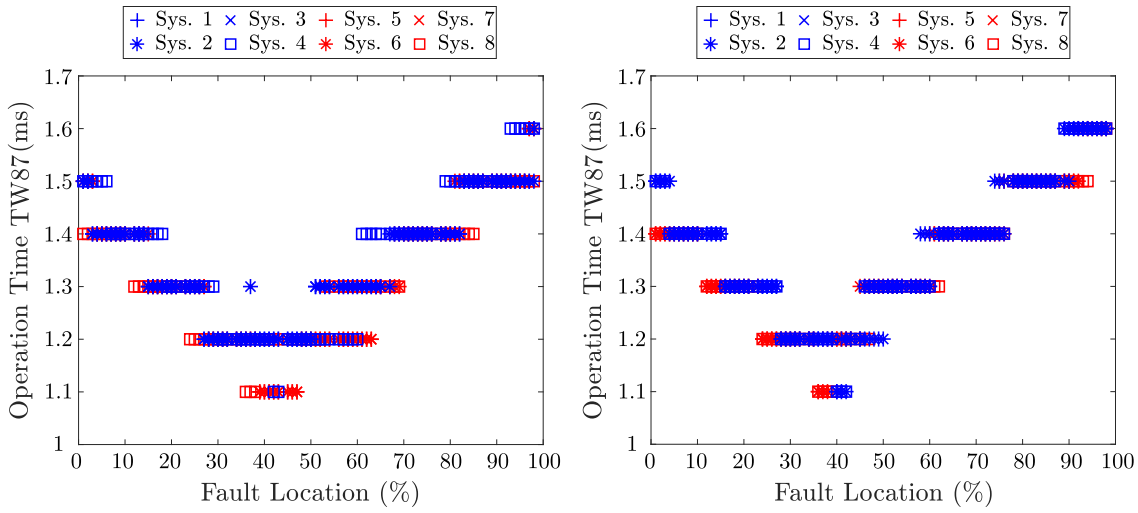

(a) AG Fault (b) BC Fault

Source: own authorship.

TW87 presents a different pattern than the others elements, in such a way that, instead of increasing the operation time along with the fault distance, it first decreases the tripping time until half the line length, approximately, than starts to increase as the fault moves away from the reference terminal. The operation time stays between 1.1 and 1.7 ms approximately in the analyzed system.

In this part of the study, the probability density of the operation time of each protection element is analyzed and depicted in Figures 6.27, 6.28, 6.29 and 6.30, in which the dashed lines represent systems modeled as Be while the continuous lines represent the JM systems. Besides,

Figure 6.27. TD21 distribution probability of operation time (ms).

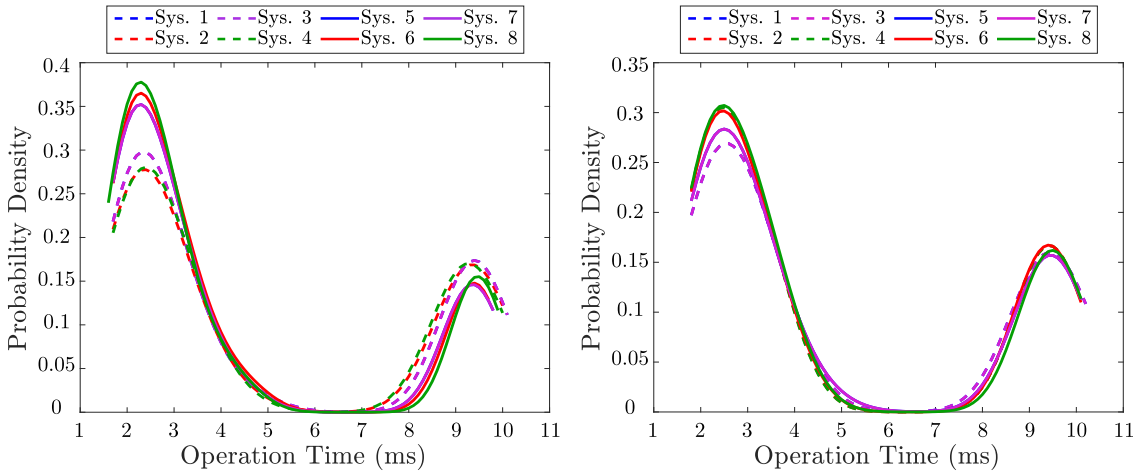

(a) AG Fault (b) BC Fault

Source: own authorship.

Figure 6.28. TD32 distribution probability of operation time (ms).

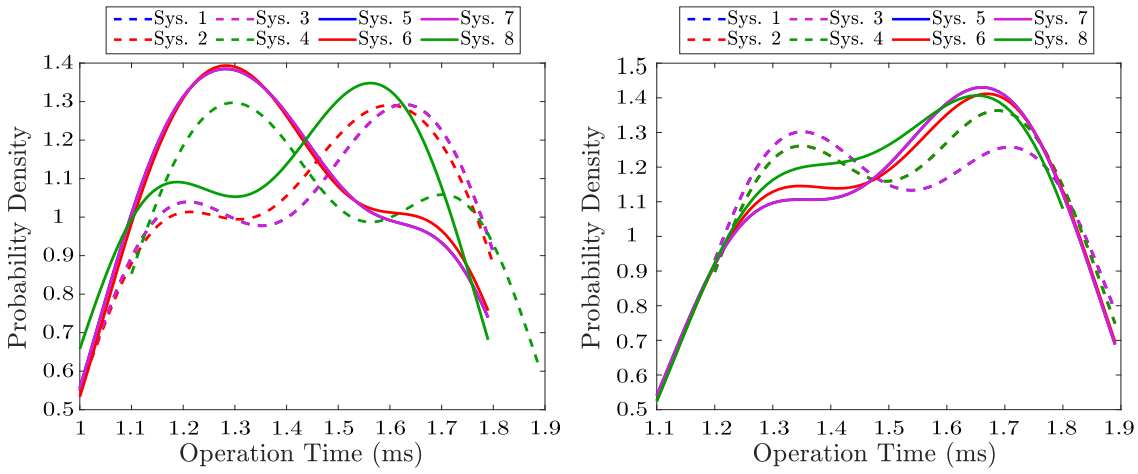

(a) AG Fault (b) BC Fault

Source: own authorship.

in all figures, System 1 and 5 (represented by the blue dashed and continuous lines, respectively) are overlapped by System 3 and 7, proving that the probability density of operation time from systems modeled as Be or JM for IdT and HS models do not affect the protection functions when only the soil characteristics are changed for NHS.

Figure 6.27 illustrates the operation time probability density for the TD21 function, verifying that most cases display an operation time up to 4 ms and few events between 8 and 10 ms approximately, as expected from the previous analysis. It is also noticed in Figure 6.27(a) that for Be lines when the operation time is smaller (i.e. faster tripping time), the probability

Figure 6.29. TW32 distribution probability of operation time (ms).

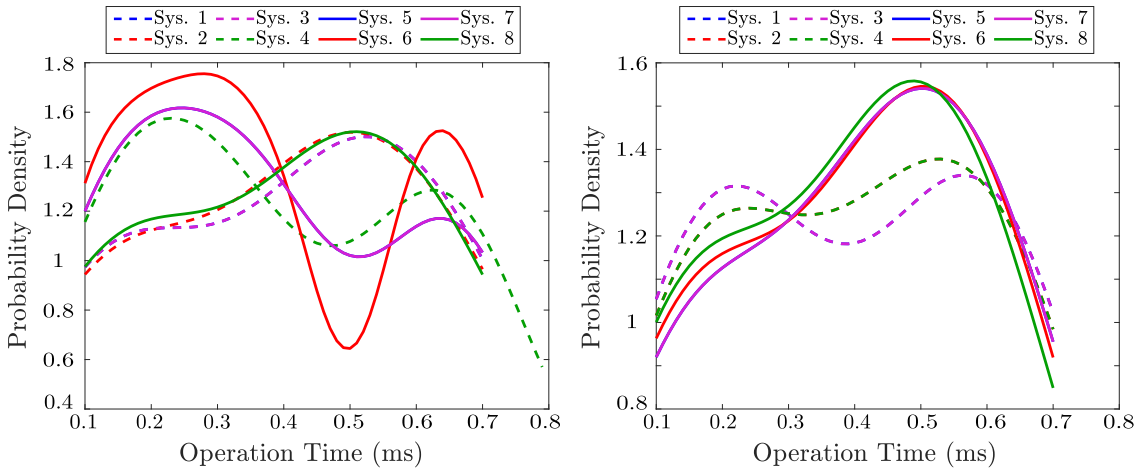

(a) AG Fault (b) BC Fault

Source: own authorship.

Figure 6.30. TW87 distribution probability of operation time (ms).

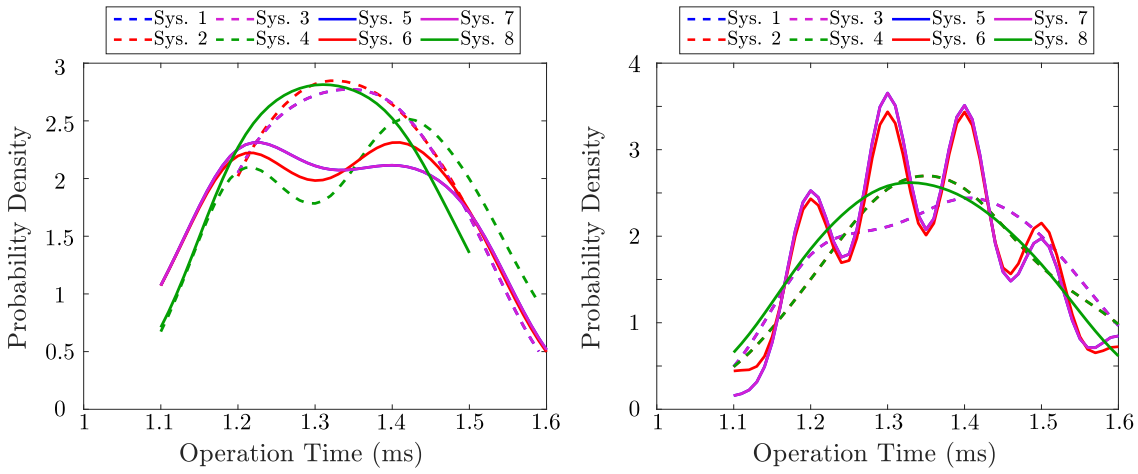

(a) AG Fault (b) BC Fault

Source: own authorship.

density is lower than for JM, while for larger operation time (slower tripping time), the Be probability density is higher than for JM cases.

Evaluating the probability density results for the TD32 function and comparing the AG fault cases with BC ones in Figure 6.28, larger differences in the patterns for different modeling characteristics are verified. In Figure 6.28(a), the largest density values vary in between 1.3 and 1.6 ms, depending on the system, while from Figure 6.28(b), for BC events, one can see that most curves have their highest density in between 1.6 and 1.7 ms. Despite these time differences, they are not considered relevant.

Analyzing Figure 6.29 for TW32, it is observed that the curves for single-phase-to-ground fault have a greater divergence between themselves than the curves for BC faults. Finally, evaluating the probability density for TW87, comparing Figures 6.30(a) and 6.30(b), it is noticed that for BC fault cases, the probability curves present greater variability in the patterns than for AG events. As the tripping time for TW87 is faster for faults in the middle of the line (Figure 6.26), the probability density for faster operation times is lower, while the tripping time increases as the fault moves away from the center, so the largest probability density corresponds to the middle of the graphic, as expected.

Aiming to provide further investigation on time-domain protection elements tripping time related to TL modeling approaches impact, the average operation time for each function and system are calculated and depicted in Table 6.4. From this table, it is observed that the average operation time has a tendency to decrease for JM systems, since TW present higher propagation velocity than Be, as previously evidenced. In addition, as concluded from the initial studies,

Table 6.4. Average tripping times

System	TD21 AT	TD21 BC	TD32 AT	TD32 BC	TW32 AT	TW32 BC	TW87 AT	TW87 BC
1	4.76 ms	4.98 ms	1.45 ms	1.53 ms	0.41 ms	0.40 ms	1.34 ms	1.37 ms
2	4.85 ms	4.74 ms	1.45 ms	1.53 ms	0.40 ms	0.40 ms	1.34 ms	1.37 ms
3	4.76 ms	4.98 ms	1.45 ms	1.53 ms	0.41 ms	0.40 ms	1.34 ms	1.37 ms
4	4.83 ms	4.73 ms	1.46 ms	1.53 ms	0.39 ms	0.40 ms	1.36 ms	1.37 ms
5	4.15 ms	4.77 ms	1.41 ms	1.52 ms	0.38 ms	0.40 ms	1.32 ms	1.36 ms
6	4.09 ms	4.74 ms	1.41 ms	1.52 ms	0.38 ms	0.40 ms	1.33 ms	1.35 ms
7	4.15 ms	4.77 ms	1.41 ms	1.52 ms	0.38 ms	0.40 ms	1.32 ms	1.36 ms
8	4.07 ms	4.65 ms	1.41 ms	1.51 ms	0.40 ms	0.39 ms	1.32 ms	1.35 ms

the first wavefronts present similar amplitude and arrival times for all systems, so that it is not expected to obtain larger and relevant impacts on protection functions. Even so, one must recognize that in some particular systems, operation times presented differences, highlighting that EMTP modeling strategies can affect the results of time-domain functions, but not in a relevant way.

CHAPTER 7

CONCLUSIONS AND FUTURE WORKS

This thesis presented a massive analysis of TL modeling characteristics in EMTP platforms in order to verify the impact of different models on TW propagation patterns and the respective effects on well known TWFL methods and time-domain protection functions performance. Especially for TW phenomenon, there is a gap in the literature related to this topic, so that researchers commonly use different modeling aspects in their works without knowing possible effects on the evaluated methods. Thus, the presented study had as main motivation the need for studies to identify relevant impacts that each line modeling strategy can have on time-domain protection and fault location functions.

Two sets of case studies were performed with the purpose to firstly identify which and how line characteristics affect the TW propagation patterns. Such studies were performed by EMTP simulations, considering different scenarios, namely: frequency-dependent and independent line model; TL ideally transposed, non-transposed and with real transposition schemes; and soil with a homogeneous resistivity along the line. In addition, the second set of studies had the purpose to verify which line characteristics pose uncertainties for the accuracy and performance of fault location and protection functionalities available in real time-domain relay. Therefore, for these evaluations, the power systems scenarios were simulated accounting for frequency-dependent and independent line model; TL ideally transposed and with real transposition schemes; and soil with homogeneous and heterogeneous resistivity along the line.

From the first analysis, it was concluded that JM model generates more attenuated and dispersed TW, resulting in TW very similar to those observed in real-world fault records. As result, JMarti model is considered more accurate for TW studies than the Bergeron model. However, no relevant loss of accuracy was verified when only the first incident aerial mode TW is considered, being the most relevant discrepancies verified for studies regarding ground mode TW and reflected/transmitted TW from/through the fault point. In addition, it is

demonstrated that the ground mode TW propagation speed is more affected along the frequency spectrum than the aerial mode, what explain why systems modeled as Be originate ground TW with slow propagation speed than JM. Hence, this great difference in the propagation velocity between aerial and ground mode for Be model results in false peaks in phase signals that insert uncertainties in the TW studies. Consequently, JM model is indicated whenever reflected, refracted and ground mode TW are under investigation. Finally, it is demonstrated that soil resistivity affect modal TW patterns, mainly ground mode ones.

From the second set of studies, results for double-phase and single-phase-to-ground fault were obtained considering computational simulations and a real time-domain protective relay. First a total of 512 fault cases were investigated considering four TWFL techniques accounting for computational applications. From the obtained results, it was concluded that, compared to the most simplified system models evaluated in this work, power systems implemented in a more detailed way tend to increase the TWFL errors. It was also verified that the TWFL methods which do not require settings based on line parameters are indeed more reliable, presenting smaller errors than classical parameter-dependent solutions. However, these techniques require the detection of TW reflected from the fault point, which is still a challenging task, specially for faults involving the ground due to the mixing mode phenomenon.

Scatter plots and boxplots were presented to analyze the influence on functions of, mainly, the two line characteristics that consisted in the most relevant sources of errors for the TWFL methods, namely: frequency-dependent line models and real transposition schemes. The results demonstrate how TWFL techniques can be affected by different line modeling strategies, pointing out that some features that can favor or jeopardize the TWFL accuracy. Hence, when TWFL methods are under investigation the recommended is modeling the systems with characteristics closer to the real ones, i.e., consider the frequency-dependence (JM); the soil with heterogeneous resistivity (NHS); and a real transposition (T). So then, the obtained results for test purposes is going to be more accurate.

Aiming validate and complement the above studies and results, 1,584 fault scenarios were simulated to generate COMTRADE files which were played back into the analyzed real time-domain relay. The previous results obtained for the TWFL methods simulations were validated by considering the relay response, demonstrating the importance of combining more than one

TWFL methods when the SETWFL technique is applied. Indeed, due to the uncertainties generated by the recognition of the reflected TW and the problem caused by the mixing mode in grounded faults, single-ended TWFL approaches have difficulties to operate, whereas no relevant difficulties were verified in Z-based fault location methods application.

Finally, accounting for protection elements, TD21, TD32, TW32 and TW87, no relevant impact on sensibility analysis on the performance of each function were identified, since these functions depend only on the recognition of polarities, magnitudes, and voltage and current signal incremental loop. Besides, when necessary, the relay analyzes only the first incident aerial mode TW, which is not relevantly affected by the model characteristics assessed in this thesis. Hence, accounting for these time-domain protection functions, the implementation of a TL with more simplified characteristics can be used without significant loss of accuracy, unlike the TWFL methods.

Given the evaluated aspects, it is possible to propose improvements that can be addressed on future researches. Therefore, as a continuation of this work, it is suggested:

- Perform the same studies considering parallel transmission lines;
- Evaluate the impact of TL modeling characteristics varying the fault resistivity;
- Parameterize the relay with the most simplified power system model settings for all the systems in order to analyze possibles impacts when the relay is not set with accurate parameters;
- Additional comparisons with more real-world fault records;
- Study on the impact of filtering methods on TW- and phasor-based fault location approaches;
- Ground mode transient analysis in real systems, verifying its impacts on fault location and protection methods;
- Parametric investigation and analysis on wave dispersion for different conductors and tower configuration;
- Assessment of the impacts of interferences and noises on methods available in real line monitoring devices.

REFERENCES

ARAUJO, A.; NEVES, W. *Cálculo de transitórios eletromagné*. [S.l.: s.n.]. Cited in page 14.

BEWLEY, L. V. Traveling waves on transmission systems. *Transactions of the American Institute of Electrical Engineers*, v. 50, n. 2, p. 532–550, 1931. Cited 4 times in pages 8, 10, 13, and 16.

CHALANGAR, H.; OULD-BACHIR, T.; SHESHYEKANI, K.; LI, S.; MAHSEREDJIAN, J. Evaluation of a constant parameter line-based twfl real-time testbed. *IEEE Transactions on Power Delivery*, v. 35, n. 2, p. 1010–1019, 2020. Cited in page 38.

CHAMIA, M.; LIBERMAN, S. Ultra high speed relay for ehv/uhv transmission lines – development, design and application. *IEEE Transactions on Power Apparatus and Systems*, PAS-97, n. 6, p. 2104–2116, 1978. Cited 3 times in pages 9, 10, and 12.

CLARKE, E. *Circuit Analysis of A-C Power Systems; Symmetrical and Related Components*. Wiley, 1943. (Circuit Analysis of A-C Power Systems; Symmetrical and Related Components, v. 1). Disponível em: <https://books.google.com.br/books?id=zR4hAAAAMAAJ>. Cited in page 17.

COSTA, F. B.; SOBRINHO, A. H. P.; ANSALDI, M.; ALMEIDA, M. A. D. The effects of the mother wavelet for transmission line fault detection and classification. In: *Proceedings of the 2011 3rd International Youth Conference on Energetics (IYCE)*. [S.l.: s.n.], 2011. p. 1–6. Cited in page 15.

CROSSLEY, P.; MCLAREN, P. Distance protection based on travelling waves. *IEEE Transactions on Power Apparatus and Systems*, PAS-102, n. 9, p. 2971–2983, 1983. Cited 2 times in pages 10 and 12.

DAS, S.; SANTOSO, S.; GAIKWAD, A.; PATEL, M. Impedance-based fault location in transmission networks: theory and application. *IEEE Access*, v. 2, p. 537–557, 2014. Cited in page 7.

DEMAGALHAESJUNIOR, F. M.; LOPES, F. V. Mathematical study on traveling waves phenomena on three phase transmission lines part ii: Reflection and refraction matrices. *IEEE Transactions on Power Delivery*, p. 1–1, 2021. Cited in page 46.

DOMMEL, H. W. Digital computer solution of electromagnetic transients in single-and multiphase networks. *IEEE Transactions on Power Apparatus and Systems*, PAS-88, n. 4, p. 388–399, 1969. Cited in page 32.

DOMMEL, H. W. *Electromagnetic Transients Program Reference Manual (EMTP Theory Book)*. [S.l.]: Portland (OR, USA): Bonneville Power Administration, 1986. Cited in page 32.

DOMMEL, H. W.; MICHELS, J. M. High speed relaying using traveling wave transient analysis. *IEEE Power Engineering Society Winter Meeting, IEEE*, New York, USSA, A78, 02 1978. Cited 2 times in pages 10 and 12.

DZIENIS, C.; KEREIT, M.; BLUMSCHEIN, J.; CLAUS, M. An experimental analysis of high-speed-distance protection. In: *2010 Modern Electric Power Systems*. [S.l.: s.n.], 2010. p. 1–8. Cited 2 times in pages 11 and 12.

EMPRESA DE PESQUISA ENERGÉTICA. *Plano Decenal de Expanção de energia*. [S.l.], 2021. (in Portuguese). Cited in page 1.

FENG, Z.; JUN, L.; LI, Z.; ZHIHAO, Y. A new fault location method avoiding wave speed and based on traveling waves for ehv transmission line. In: *2008 Third International Conference on Electric Utility Deregulation and Restructuring and Power Technologies*. [S.l.: s.n.], 2008. p. 1753–1757. Cited 2 times in pages 8 and 12.

FINNEY, D.; ZHANG, Z.; CARDENAS, J. Ultra fast distance protection. In: *10th IET International Conference on Developments in Power System Protection (DPSP 2010). Managing the Change*. [S.l.: s.n.], 2010. p. 1–5. Cited 2 times in pages 11 and 12.

GALE, P. F.; CROSSLEY, P. A.; BINGYIN, X.; YAOZHONG, G.; CORY, B. J.; BARKER, J. R. G. Fault location based on travelling waves. In: *1993 Fifth International Conference on Developments in Power System Protection*. [S.l.: s.n.], 1993. p. 54–59. Cited 5 times in pages 8, 12, 23, 24, and 25.

GENERAL ELECTRIC. *L60 Line Phase Comparison System*. [S.l.], 2009. Disponível em: <https://www.gegridsolutions.com/multilin/catalog/l60.htm>. Cited in page 2.

GILANY, M.; IBRAHIM, D. k.; ELDIN, E. S. T. Traveling-wave-based fault-location scheme for multiend-aged underground cable system. *IEEE Transactions on Power Delivery*, v. 22, n. 1, p. 82–89, 2007. Cited 4 times in pages 8, 12, 23, and 25.

GIRGIS, A.; HART, D.; PETERSON, W. A new fault location technique for two- and three-terminal lines. *IEEE Transactions on Power Delivery*, v. 7, n. 1, p. 98–107, 1992. Cited 2 times in pages 7 and 12.

GLOVER, J. D.; SARMA, M. S.; OVERBYE, T. J. *Power System Analysis and Design;*. 5. ed. [S.l.]: CENGAGE Learning, 2011. Cited in page 3.

Greenwood, A. *Electrical Transients in Power Systems*. Wiley, 1971. ISBN 9780471326502. Disponível em: <https://books.google.com.br/books?id=9-4iAAAAMAAJ>. Cited in page 16.

Guzmán, A.; Kasztenny, B.; Tong, Y.; Mynam, M. V. Accurate and economical traveling-wave fault locating without communications. In: *2018 71st Annual Conference for Protective Relay Engineers (CPRE)*. [S.l.: s.n.], 2018. p. 1–18. Cited in page 29.

HE, Z.; MAI, R.; HE, W.; QIAN, Q. Phasor-measurement-unit-based transmission line fault location estimator under dynamic conditions. *Generation, Transmission and Distribution, IET*, v. 5, p. 1183–1191, 11 2011. Cited 2 times in pages 7 and 12.

III SCHWEITZER, E. O.; GUZMAN-CASILLAS, A.; KASZTENNY, B. Z.; TONG, Y.; MYNAM, M. V. *Traveling wave based single end fault location*. [S.l.]: Patent Application Publication, 2019. US Patent 10,295,585. Cited in page 29.

IRWIN, J.; NELMS, R. *Basic Engineering Circuit Analysis*. John Wiley & Sons, 2010. (Wiley Plus Products Series). ISBN 9780470633229. Disponível em: <https://books.google.com.br/books?id=E4O662eBIu8C>. Cited in page 18.

IZYKOWSKI, J.; ROSOLOWSKI, E.; BALCEREK, P.; FULCZYK, M.; SAHA, M. Fault location on double-circuit series-compensated lines using two-end unsynchronized measurements. *IEEE Transactions on Power Delivery - IEEE TRANS POWER DELIVERY*, v. 26, p. 2072–2080, 10 2011. Cited 2 times in pages 7 and 12.

JOHNS, A.; JAMALI, S. Accurate fault location technique for power transmission lines. In: . [S.l.: s.n.], 1990. v. 137, n. 6, p. 395–402. Cited 2 times in pages 7 and 12.

LANZ, O.; HANGGLI, M.; BACCHINI, G.; ENGLER, F. Transient signals and their processing in an ultra high-speed directional relay for ehv/uhv transmission line protection. *IEEE Transactions on Power Apparatus and Systems*, PAS-104, n. 6, p. 1463–1473, 1985. Cited 2 times in pages 10 and 12.

LEUVEN, E. C. *ATP-alternative transiente program- rule book*. [S.l.]: Herverlee, Belgium, 1987. Cited in page 32.

LOPES, F.; HONORATO, T.; RIBEIRO, J. P.; SILVA, K. Parametric sensitivity analysis of actual transmission line time-domain protection relay. In: . [S.l.: s.n.], 2020. p. 128 (6 pp.)–128 (6 pp.). Cited 3 times in pages 19, 21, and 54.

LOPES, F.; JOÃ£O, P.; RIBEIRO, J. P.; JR, E. L.; SILVA, K. Parametric analysis of the travelling wave-based differential protection tw87. *The Journal of Engineering*, v. 2018, p. 1297 – 1302, 10 2018. Cited in page 2.

LOPES, F. V. *Localização de faltas em tempo real baseada na teoria de ondas viajantes usando dados não sincronizados de dois terminais*. Tese (Doutorado), 05 2014. (in Portuguese). Cited in page 6.

LOPES, F. V. Settings-free traveling-wave-based earth fault location using unsynchronized two-terminal data. *IEEE Transactions on Power Delivery*, v. 31, n. 5, p. 2296–2298, 2016. Cited 2 times in pages 9 and 12.

LOPES, F. V.; DANTAS, K. M.; SILVA, K. M.; COSTA, F. B. Accurate two-terminal transmission line fault location using traveling waves. *IEEE Transactions on Power Delivery*, v. 33, n. 2, p. 873–880, 2018. Cited 5 times in pages 9, 12, 23, 26, and 44.

LOPES, F. V.; FERNANDES, D.; NEVES, W. L. A. A traveling-wave detection method based on park's transformation for fault locators. *IEEE Transactions on Power Delivery*, v. 28, n. 3, p. 1626–1634, 2013. Cited in page 15.

LOPES, F. V.; JR., E. J. S. L.; RIBEIRO, J. P. G.; LOPES, L.; PIARDI, A.; OTTO, R.; NEVES, W. Using the differentiator-smoother filter to analyze traveling waves on transmission lines: Fundamentals, settings and implementation. In: *International Conference on Power Systems Transients (IPST 2019)*. Perpignan, France: [s.n.], 2019. Cited 3 times in pages 13, 14, and 15.

LOPES, F. V.; LIMA, P.; RIBEIRO, J. P. G.; HONORATO, T. R.; SILVA, K. M.; LEITE, E. J. S.; NEVES, W. L. A.; ROCHA, G. Practical methodology for two-terminal traveling wave-based fault location eliminating the need for line parameters and time synchronization. *IEEE Transactions on Power Delivery*, v. 34, n. 6, p. 2123–2134, 2019. ISSN 0143-7046. Cited 4 times in pages iv, 38, 39, and 44.

MAGALHAESJR, F. M.; LOPES, F. V. Mathematical study on traveling waves phenomena on three phase transmission lines part ii: Reflection and refraction matrices. *IEEE Transactions on Power Delivery*, p. 1–1, 2021. Cited in page 24.

MARTI, J. R. Accurate modelling of frequency-dependent transmission lines in electromagnetic transient simulations. *IEEE Transactions on Power Apparatus and Systems*, PAS-101, n. 1, p. 147–157, 1982. Cited in page 32.

MARTINS-BRITTO, A. *Realistic Modeling of Power Lines for Transient Electromagnetic Interference Studies*. Tese (Doutorado), 07 2020. Cited in page 3.

OPERADOR NACIONAL DO SISTEMA ELÉTRICO. *Relatório de Aná de perturbação-RAP*. [S.l.], 2020. (in Portuguese). Cited in page 1.

OPERADOR NACIONAL DO SISTEMA ELÉTRICO. *Procedimentos de Rede - Submódulo 2.11: Requisitos mínimos para sistemas de proteção, de registros de perturbações e de teleproteção*. [S.l.], 2021. (in Portuguese). Cited in page 2.

PERCIVAL, D. B.; WALDEN, A. T. *Wavelet methods for time series analysis*. [S.l.]: Cambridge university press, 2000. v. 4. Cited in page 15.

PHADKE, A. G.; THORP, J. S. *Computer Relaying for Power Systems*. Chichester, England: John Wiley and Sons Ltd, 2009. (Power Systems). ISBN 978-0-470-05713-1. Cited 5 times in pages 2, 13, 14, 24, and 46.

RADOJEVIC, Z.; KIM, C.-H.; POPOV, M.; PRESTON, G.; TERZIJA, V. New approach for fault location on transmission lines not requiring line parameters. 01 2009. Cited 2 times in pages 7 and 12.

RIBEIRO, E.; LOPES, F.; HONORATO, T. Modelagem do filtro differentiator-smoother: Validação via análise de transitórios e resposta em frequência de dispositivos microprocessados reais. *XIII Conferência Brasileira sobre Qualidade de Energia Elétrica (CBQEE)*, p. 1–6, 2019. (in Portuguese). Cited in page 15.

RIBEIRO, E. P. A.; LOPES, F. V.; RIBEIRO, J. P. G.; LEITE, E. J. S. Atp/models differentiator-smoother filter model validated using actual time-domain relay. In: *2018 Workshop on Communication Networks and Power Systems (WCNPS)*. [S.l.: s.n.], 2018. p. 1–4. Cited in page 13.

RIBEIRO, J. P. *Estudo e Avaliação das Funções de Proteção de Linhas de Transmissão Aplicadas no Domío do Tempo Disponíveis no Relé SEL-T400L*. Dissertação (Mestrado), 12 2019. (in Portuguese). Cited in page 18.

RIBEIRO, J. P. G.; LOPES, F. V. Modelling and simulation of a time-domain line protection relay. *The Journal of Engineering*, v. 2018, n. 15, p. 861–865, 2018. Cited in page 2.

SAHA, M.; IZYKOWSKI, J.; ROSOLOWSKI, E. Atp-emtp study of current differential protection with synchronization and fault location functions. In: *International Conference on Power Systems Transients*. Vancouver, Canada: [s.n.], 2013. Cited 2 times in pages 7 and 12.

SAHA, M. M.; IZYKOWSKI, J. J.; ROSOLOWSKI, E. *Fault Location on Power Networks*. 1st. ed. [S.l.]: Springer Publishing Company, Incorporated, 2009. ISBN 1848828853. Cited 4 times in pages 2, 6, 8, and 15.

SALIM, R.; SALIM, K.; BRETAS, A. Further improvements on impedance-based fault location for power distribution systems. *Generation, Transmission and Distribution, IET*, v. 5, p. 467 – 478, 05 2011. Cited 2 times in pages 7 and 12.

SCHWEITZER; KASZTENNY, B.; GUZMAN, A.; SKENDZIC, V.; MYNAM, M. Speed of line protection - can we break free of phasor limitations? October 2014. Cited 5 times in pages 8, 9, 11, 12, and 18.

SCHWEITZER, E.; KASZTENNY, B.; MYNAM, M.; GUZMAN, A.; FISCHER, N.; SKENDZIC, V. Defining and measuring the performance of line protective relays. In: *Western Protective Relay Conference*. [S.l.: s.n.], 2016. Cited in page 44.

SCHWEITZER, E. O.; GUZMÁN, A.; MYNAM, M. V.; SKENDZIC, V.; KASZTENNY, B.; MARX, S. Locating faults by the traveling waves they launch. In: *2014 67th Annual Conference for Protective Relay Engineers*. [S.l.: s.n.], 2014. p. 95–110. Cited 4 times in pages 2, 13, 15, and 17.

SCHWEITZER, E. O.; KASZTENNY, B.; MYNAM, M. V. Performance of time-domain line protection elements on real-world faults. In: *2016 69th Annual Conference for Protective Relay Engineers (CPRE)*. [S.l.: s.n.], 2016. p. 1–17. Cited 9 times in pages 2, 11, 15, 19, 20, 21, 22, 23, and 30.

SCHWEITZER ENGINEERING LABORATORIES. *Ultra-High-Speed Transmission Line Relay Traveling-Wave Fault Locator High-Resolution Event Recorder*. [S.l.], 2019. Disponível em: <https://selinc.com/products/T400L/>. Cited 12 times in pages 2, 11, 19, 20, 21, 22, 23, 24, 26, 27, 30, and 54.

SIDWALL, K.; FORSYTH, P. Advancements in real-time simulation for the validation of grid modernization technologies. *Energies*, v. 13, p. 4036, 08 2020. Cited in page 3.

TAKAGI, T.; BARBAR, J.; KATSUHIKO, U.; SAKAGUCHI, T. Fault protection based on travelling wave theory, part i: Theory. *IEEE Power Engineering Society Summer Meeting*, IEEE, Paper A77, July. 1977. Cited 2 times in pages 10 and 12.

TAKAGI, T.; YAMAKOSHI, Y. .; YAMAURA, M.; KONDOW, R.; MATSUSHIMA, T. Development of a new type fault locator using the one-terminal voltage and current data. *IEEE Transactions on Power Apparatus and Systems*, PAS-101, n. 8, p. 2892–2898, 1982. Cited 3 times in pages 6, 7, and 12.

TAKAGI, T.; YAMAKOSI, Y.; YAMAURA, M.; KONDOW, R.; MATSUSHIMA, T.; MASUI, M. Digital differential relaying system for transmission line primary protection using traveling wave theory — its theory and field experience. *IEEE Power Engineering Society Winter Meeting*, IEEE, Paper A79, 1979. Cited 2 times in pages 10 and 12.

TLEIS, N. (Ed.). *Power Systems Modelling and Fault Analysis (Second Edition)*. Second edition. Academic Press, 2019. ISBN 978-0-12-815117-4. Disponível em: <https://www.sciencedirect.com/science/article/pii/B9780128151174000138>. Cited in page 1.

TZIOUVARAS, D.; ROBERTS, J.; BENMOUYAL, G. New multi-ended fault location design for two- or three-terminal lines. In: *2001 Seventh International Conference on Developments in Power System Protection (IEE)*. [S.l.: s.n.], 2001. p. 395–398. Cited 2 times in pages 7 and 12.

VITINS, M. A fundamental concept for high speed relaying. *IEEE Transactions on Power Apparatus and Systems*, PAS-100, n. 1, p. 163–173, 1981. Cited 2 times in pages 10 and 12.

ZIMATH, S. L.; RAMOS, M. A. F.; FILHO, J. E. S. Comparison of impedance and travelling wave fault location using real faults. In: *IEEE PES T D 2010*. [S.l.: s.n.], 2010. p. 1–5. Cited 3 times in pages 2, 15, and 52.